universität wien

MASTERARBEIT / MASTER'S THESIS

Titel der Masterarbeit / Title of the Master's Thesis

„Effects of photocatalytic TiO_2 nanoparticles on Molecular Weight and Elemental Distribution of Natural Organic Matter"

verfasst von / submitted by

Claudia Gonzalez

angestrebter akademischer Grad / in partial fulfilment of the requirements for the degree of

Master of Science (MSc)

Wien, 2016 / Vienna 2016

Studienkennzahl lt. Studienblatt / degree programme code as it appears on the student record sheet:	A 066 299
Studienrichtung lt. Studienblatt / degree programme as it appears on the student record sheet:	Interdisziplinäres Masterstudium Environmental Sciences
Betreut von / Supervisor:	Univ.-Prof. Dr. Thilo Hofmann
Mitbetreut von / Co-Supervisor:	Dr. Frank von der Kammer

Abstract

The increase of natural organic matter (NOM) in aquatic environments affects the quality of drinking water sources. It also affects the efficiency of the disinfection treatment processes and the formation potential of harmful by-products.

Innovative techniques have been applied to remove NOM from raw water, but the efficiency of these techniques to remove low molecular weight (LMW) compounds is still under examination.

Since LMW compounds play a role in the formation of new disinfection by-products (DBPs), removal techniques, such as advance oxidation processes, have to be evaluated in order to understand and predict the reactivity of the residual organic characteristics of NOM after photocatalytic treatment.

For a more complete evaluation, it is necessary to apply as many independent analytical methods as possible that deal with the NOM complexity.

In this thesis, photocatalytic TiO_2 nanoparticles are used to degrade a commercial standard Pahokee Peat humic acid (PPHA). The changes induced in the PPHA are monitored using a HPSEC-UV/Vis-Fluorescence-ICP-MS system, as well as a UV/Vis Spectrophotometer and a Spectrofluorometer to complement the analysis.

An equilibrium experiment (Time study), photocatalytic TiO_2 activity and Adsorption Isotherm study were performed previous to the Irradiation experiment in order to set the experimental conditions.

The results of this study confirm that the photocatalytic activity of TiO_2 nanoparticles degrades PPHA molecules from high molecular weight to LMW compounds.

The change in molecular weight distribution is accompanied by reductions in UV-Vis absorbance, with a change of absorbance ratios that points to a loss of

aromaticity and reduction of formation potential of DBPs. Fluorescence and elemental distribution are also affected by the photocatalytic degradation. However, the extent of degradation is not related to the concentrations of TiO_2 nanoparticles, but to the adsorption of PPHA onto the surface of TiO_2.

Zusammenfassung

Der Anstieg an natürlichem organischem Material (natural organic matter, NOM) in aquatischen Umgebungen beeinflusst die Qualität von Trinkwasserquellen. Zusätzlich beeinflusst dieser Anstieg die Effektivität von Desinfektionsprozessen und die Wahrscheinlichkeit der Entstehung schädlicher Nebenprodukte. Innovative Methoden wurden zur Entfernung von NOM aus Nutzwasser angewandt, doch die Effektivität dieser Methoden in der Entfernung von Verbindungen mit niedrigem molekularem Gewicht (low molecular weight, LMW) wird noch untersucht.

Da LMW Verbindungen eine Rolle in der Bildung neuer Nebenprodukte bei Desinfektionsprozessen (disinfection by-products, DBPs) spielen, müssen Methoden zur Entfernung, wie etwa erweiterte Oxidation (advanced oxidation processes, AOPs), evaluiert werden. Diese Evaluierung ist notwendig, um die Reaktivität der remanenten organischen Eigenschaften von NOM nach Anwendung photokatalytischer Verfahren zu verstehen und zu prognostizieren. Für eine vollständigere Evaluierung erweist sich die Anwendung verschiedener, unabhängiger analytischer Methoden als notwendig, die die Komplexität von NOM behandeln.

In dieser Arbeit werden TiO_2 Nanopartikel verwendet, um kommerzielle Standard Pehokee Peat Huminsäure (Pahokee Peat humic acid, PPHA) abzubauen. Die herbeigeführten Veränderungen der PPHA werden durch ein HPSEC-UV/Vis-Fluoreszenz-ICP-MS System beobachtet. Zusätzlich werden ein UV/Vis Spectrophotometer und ein Spectrofluorometer zur Analyse verwendet. Ein Equilibrium-Experiment (Zeitstudie) sowie eine Untersuchung der photokatalytischen TiO_2 Aktivität und der Adsorptionsisotherme wurden vor dem Irradiations-Experiment durchgeführt, um die experimentellen Gegebenheiten festzustellen.

Die Ergebnisse dieser Studie bekräftigen, dass die photokatalytische Aktivität von TiO_2 Nanopartikeln PPHA Moleküle mit hohem molekularem Gewicht (high molecular weight, HMW) zu LMW Verbindungen abbaut. Die Veränderung in der Verteilung des molekularen Gewichts wird begleitet von einer Reduktion der

UV-Vis Absorption. Die Änderung der Absorptionsraten deutet auf eine Verringerung der Aromatizität und eine reduzierte Wahrscheinlichkeit der Entstehung von DBPs hin. Fluoreszenz und Element-Verteilung werden ebenfalls von photokatalytischem Abbau beeinflusst. Allerdings steht das Ausmaß der Degradation nicht im Zusammenhang mit der Konzentration von TiO_2 Nanopartikeln, sondern mit der Adsorption von PPHA an der Oberfläche von TiO_2.

Contents

List of Figures

List of tables

1. Introduction

Natural Organic Matter (NOM) is generally defined as a mixture of particulate and dissolved organics generated by the microbial decay of biological material, whose characteristics vary from one water source to another. It has a wide range of distributions in molecular weight (MW) and functional groups (phenolic, hydroxyl, and carboxyl groups), which originate from allochthonous (e.g., terrestrial and vegetative debris) and autochthonous (e.g., algae) inputs (Cui & Choo, 2014).

The presence of NOM has a significant impact to the quality of drinking water sources (Matilainen et al. 2010). The main concern with the presence of NOM is the formation of disinfectant by-products (DBPs) from disinfection process, mainly chlorination, during drinking water treatment (Ibrahim & Aziz, 2014).

Even though the use of alternative disinfectants such as ozone, chlorine dioxide and chloramine was able to reduce major DBPs formed by chlorine, they formed its specific DBPs (Ibrahim & Aziz, 2014; Lu et al., 2009). The DBPs most commonly detected in drinking water are trihalomethanes (THMs) and haloacetic acids (HAAs), and certain DBPs such as Chloroform, Dichlorobromomethane and Trichloroacetic acid are potentially carcinogen to human.

Other disadvantages of NOM to drinking water sources and treatment processes are, that it:

- acts as a mobile carrier to inorganic and organic pollutants (increase of transportation and distribution)
- competes with other pollutants for adsorption sites
- causes yellow/brown coloration of the water, as well as flavor and odor problems
- serves as a substrate to undesirable biological growth in the distribution system
- controls coagulant and disinfectant dosage which cause an increase of sludge volumes and formation of DBPs

- causes membrane fouling (Ibrahim & Aziz, 2014).

A significant fraction of NOM is composed of humic substances, which are colored high-molecular weight substances. They form small aggregates on a specific surface, where water and other molecules, as well as ions, can be taken up reversibly (Kördel et al., 1997).

According to their behavior in aqueous solution at different pH-values, humic substances are mainly divided in: fulvic acids (water soluble at acidic to alkaline pH), humic acids (insoluble at acidic pH), and humin (insoluble). Many studies have used humic acids (HAs) as model compound because its heterogeneous nature resembles that of natural waters (Uyguner & Bekbolet, 2005).

Currently, several techniques have been applied to remove NOM from raw water, including coagulation, ozonation, membrane filtration and ion-exchange. Most of the NOM can be removed by coagulation, which is one of the most common and economically feasible methods, although, the hydrophilic, low molecular weight (LMW) fraction of NOM is apparently removed less efficiently than the hydrophobic, high molecular weight (HMW) compounds (Matilainen et al., 2011).

Present knowledge and experience show that the hydrophobic, HMW, with high aromatic carbon content, are the most important precursors for the formation of DBPs after chlorination. Hydrophilic, LMW however may play a role in the formation of new compounds during disinfection, since bromine and iodine have been noted to be more reactive with this fraction in the formation of THMs and HAAs (Chen et al., 2008). Since LMW tends to be less removed, treatments should focus on the removal of this part of NOM.

More recently, advanced oxidation processes (AOP), which involve the generation of highly reactive hydroxyl radicals ($HO^{\cdot}$), have emerged as a promising water and wastewater treatment technology for degradation or mineralization of a wide range of organic contaminants, including NOM.

A class of AOP employs photocatalysis using Titanium Dioxide (TiO_2) as a photocatalyst, which is one of the most attractive processes because of its low-cost,

environmental friendly, and almost complete destruction of humic acid molecules by the direct oxidation process (Pansamut et al., 2013). Because of its high specific surface area and sorption capacity for ionic and nonionic species, the use of nano-TiO_2 has been promoted as a scavenger of inorganic and organic contaminants in water treatment plants and in the remediation of polluted subsurface environments (French et al., 2009).

When a photocatalytic surface is illuminated by light with energy equal to or larger than the bandgap energy (3.03 eV for TiO_2), it excites the electrons in the valance band to the conduction band, resulting in the formation of a positive hole (h^+) in the valance band (VB) and an electron (e^-) in the conduction band (CB). The positive hole oxidizes either pollutants directly or water to produce $HO^{\cdot}$ radicals, whereas the electron in the conduction band reduces oxygen adsorbed to TiO_2,

$$TiO_2 + hv\ (\geq 3.03eV) \rightarrow e^-_{(CB)} + h^+_{(VB)} \qquad (1)$$

$$h^+ + Organic \rightarrow CO_2 \qquad (2)$$

$$h^+ + H_2O \rightarrow HO^{\cdot} + H^+ \qquad (3)$$

$$HO^{\cdot} + Organic \rightarrow CO_2 \qquad (4)$$

$$e^- + O_2 \rightarrow O_2^- \qquad (5)$$

In the photocatalytic degradation of the pollutants, when the reduction process of oxygen (Eq. (5)) and the oxidation of pollutants (Eq. (2) and (4)) do not proceed simultaneously, electrons will accumulate in the conduction band, leading to a recombination of electrons and positive holes.

Therefore, efficient consumption of electrons is essential to promote photocatalytic oxidation. TiO_2 absorbs radiation below the visible range of the light spectrum. Hence, the photoactivation of TiO_2 requires radiation with light of wave-

length less than or equal to 384 nm, with an absorbance maximum at ~ 340 nm (Thiruvenkatachari et al., 2008).

This thesis studies the influence of photocatalytic TiO_2 nanoparticles on the physico-chemical characteristics of HAs under controlled conditions. Its main objective is to evaluate the molecular weight and elemental composition changes of a commercial standard humic acid (Pahokee Peat) during photocatalytic degradation, using TiO_2 nanoparticles and a solar UV-light simulator. The degradation efficiency of TiO_2 nanoparticles will be evaluated with the loss of aromaticity, molecular weight and formation potential of DBPs reduction.

HAs present in the irradiated TiO_2, go through many chain and consecutive reactions (Uyguner & Bekbolet, 2004). The photocatalytic degradation occurs via LMW organic carboxylic acids (4-hydroxybenzoic acid, oxalic acid, succinic acid, malonic acid) as reaction intermediates to water and CO_2 (Carp et al., 2004).

HAs are macromolecules with many redox centers, which participate both as electron donor centers (oxidation) and electron acceptor centers (reduction). Sequential electron transfer from excited HAs to the TiO_2 conduction band could lead to mineralization with CO_2 evolution, while the electron transfer from the TiO_2 conduction band to HAs tends to inhibit mineralization (Fig. 1):

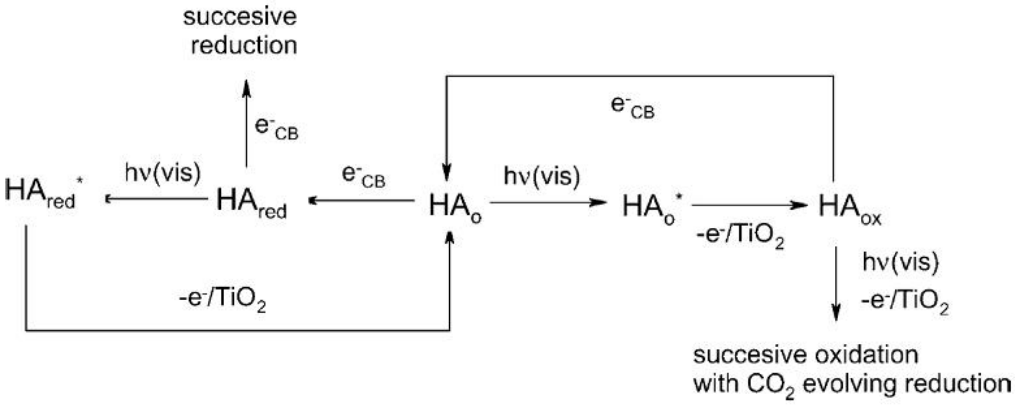

Figure 1 Sequential photoinduced electron transfer to and from TiO_2 conduction band accompanying transformation of HAs (Carp et al., 2004)

The reactions of $OH^{\cdot}$ with NOM happen in three different ways:

- by the addition of $OH^{\cdot}$ to double bonds,
- by H-atom abstraction, which yields carbon centered radicals, and
- by a reaction mechanism where $OH^{\cdot}$ gets an electron from an organic substituent (Matilainen and Sillanpää, 2010).

It is important to determine the residual organic characteristics after photocatalytic treatment, in order to assess the final products. However, there is not a single analytical tool to monitor the changes in the composition and reactivity of HAs after photocatalytic degradation, due to its heterogeneous nature (Chen et al., 2002).

To deal with HAs complexity, it is necessary to apply as many independent methods as possible to gather structural information from different points of view (Abbt-Braun et al., 2004). In this investigation, the following spectroscopic and chromatographic characterization methods will be used:

- **UV-Vis spectroscopy analysis**: Ultraviolet and visible absorption spectroscopy is the measurement of a beam of light after it passes through a sample or after reflection from a sample surface. Absorption measurements can be done at a single wavelength or over an extended spectral range. The different wavelengths are believed to identify different chromophores of NOM.

  The concentration of an analyte in a solution can be determined by measuring the absorbance at a certain wavelength applying the Beer–Lambert Law. The UV absorbance spectra of NOM decrease monotonically with increasing wavelength. Conjugated C–C multiple bonds, aromatic carbon, –COOH and –OH increase adsorption (Matilainen et al., 2011).

- **Fluorescence spectroscopy analysis**: Spectroscopic method in which the analyte molecules are excited by irradiation at a certain wavelength and the emitted radiation is measured at a specific wavelength. The specific excitation and emission wavelengths are the characteristics of a particular molecu-

lar conformation, called fluorophore. Conjugated double bonds and aromatic rings, –OH and –NH_2 enhance fluorescence, while –COOH diminishes it.

The three dimensional fluorescence excitation-emission matrix (EEM) is a technique where the spectra visualizes a range of different fluorophores covering the excitation and emission wavelengths range from ~200 nm to ~500 nm (Matilainen et al., 2011). 3D EEM has been proven to be useful for differentiating the transformation of humic substances and organic matter in natural environments (Valencia et al., 2013). Fluorescence has also been recommended as a tool for estimating the presence of biodegradable NOM, since strong correlations are found between fluorescence and biological oxygen demand values.

- **High Pressure Size-exclusion Chromatography (HPSEC)**: SEC is a fractionation method based on the molecular size. HPSEC is traditionally used for the separation of NOM, where samples are eluted over a column containing a porous gel material. Low molecular weight NOM can access more of the internal pore volume than high molecular weight NOM, which is excluded from such pores. High molecular weight NOM therefore elutes first, followed by the smaller components (Neubauer et al. 2013).

  The molecule shape and some interaction characteristics may however influence the results (Matilainen et al., 2011). HPSEC can be coupled to UV-Vis and fluorescence detection. Information on the association of metal/metalloid-NOM complexation can be obtained by coupling to UV-Vis detection and ICP-MS.

The advantages and disadvantages of the methods used are summarized in Table 1:

Table 1 Methods used to characterize different features of NOM, with their advantages and disadvantages (Matilainen et al., 2011).

Method	Advantages	Disadvantages
Fluorescence	Sensitivity, specificity, speed	Sensitive to chemical environment, e.g. pH
UV-Vis	Simple and fast, not too sophisticated instrumentation	Not all of the compounds of NOM can be detected. Wavelength specific adsorption. Under estimation of LMW compounds. Sensitive to chemical environment, e.g. pH and ionic strength
HP-SEC	Rapid, sensitive, no pre-extraction needed	Charge effects during measurement (column/NOM, eluent/NOM), choice of detector and proper standards.

2. Material and Method

2.1. Reagents

Titanium Dioxide NM-105, substance at the nanoform, was obtained from the European Commission, Joint Research Centre. As reported by the manufacturer (JRC, 2014), these nanoparticles have a primary particle size of 21 ± 9 nm, specific surface area of 47.0 ± 2.3 m^2/g, pH_{PZC} = 6.6, and purity of 99.8%.

A 10 g/L stock suspension was prepared by weighing an appropriate amount of dry powder, pre-wetting it for 24h with MilliQ water in order to achieve saturation of the particles, and dispersing it for 10 minutes in the required volume of MilliQ water, with an Ultrasonic Probe TT 13/FZ (energy input of 23.715 kJ).

Pahokee Peat reference humic acid 1R103H (PPHA) used in this study was purchased from the International Humic Substance Society (IHSS), and selected chemical data is presented in Appendix Table 4. The Pahokee peat is a typical agricultural peat soil of the Everglades formed in organic deposits from a freshwater marsh.

Stock humic acid solution was prepared by dissolving 250 mg of PPHA 1 L of MilliQ water, adjusting the pH to 8-9 in order to deprotonate COOH groups and promote dissolution. To dissolve the PPHA, the solution was gently stirred overnight at room temperature, and any undissolved PPHA was removed by filtration through a 0.2 µm Nalgene Fast PES Bottle Top filter.

The stock solution was stored in an amber glass bottle, and the DOC was measured by TOC analysis, using a Shimadzu TOC-$V_{CPH/CPN}$ with NDIR detector. The results show that the carbon concentration in the stock solution was 117.25 mg C/l. An aliquot of stock solution was taken one day before experiments for adjusting the pH to 4.5 with HCl solution 0.1 mol/L. In acidic conditions, HA can be absorbed on TiO_2 surface and react with $OH^{\cdot}$.

2.2. Methods

2.2.1. Photocatalytic activity

In order to guarantee that TiO_2 produces radicals at the chosen experimental conditions, a photocatalytic activity test was performed, since it is known that the different characteristics of TiO_2, such as particle size, crystalline structure, phase composition, BET surface area and others, have an influence on its photocatalytic activity (Tryba et al., 2007).

For the evaluation of TiO_2 photocatalytic activity, solutions containing 50, 100 and 200 mg/L of TiO_2 were mixed with 1.5 mg/L Methylene Blue (MB) solution. Solutions were kept in the dark for 30 min under shaking to equilibrate and then the irradiation of the solution. An ATLAS Suntests CPS+ with a 1.5 kW Xenon Lamp was used. For artificial sunlight (300 nm < λ < 400 nm), the light intensity striking on the surface of the reaction solution was 65 W/m^2. Aliquots were taken every five minutes, centrifuged (7000 rpm), passed through a 0.2 µm nylon filter, and the UV-Vis absorption spectrum of the clear solution was recorded with a spectrophotometer.

The decrease in absorbance value at 664 nm wavelength, corresponding to the typical peak for the absorption spectra of MB (Tryba et al., 2007), was used to determine the extent of decolorisation of MB and the photocatalytic activity of the samples with respect to irradiation time. Concentrations of MB were calculated using the calibration curve determined in advance.

2.2.2. Adsorption Isotherm experiment

In general, an adsorption isotherm is an invaluable curve describing the phenomenon governing the retention (or release) mobility of a substance from the aqueous porous media or aquatic environments to a solid-phase at a constant temperature and pH (Foo&Hameed, 2010).

Adsorption equilibrium (the ratio between the fraction adsorbed and the fraction remaining in solution) is established when an adsorbate containing phase has been in contact with the adsorbent for sufficient time, and the adsorbate concentration in the bulk solution is in a dynamic balance with the interface concentration (Foo&Hameed, 2010).

It is known that the initial adsorption kinetics of humic acids on a solid surface is rather a complex process that depends on the nature of the surface and the solution conditions (Bekbolet et al., 2002). In addition, the efficiency of the photocatalytic degradation of humic acids/NOM depends on the pre-adsorption phase for a successive interaction of the in situ generated reactive oxygen species (Uyguner-Demeril and Bekbolet, 2011).

In order to evaluate the adsorption isotherm of our system, a batch adsorption experiment was carried out in the dark in 100 ml amber glass bottles. The concentration of PPHA was 20 mg C/L at pH 4.5 and the dosage of TiO_2 varied from 0.1 to 1 g/L.

The approach of varying the concentrations of titanium dioxide instead of varying the humic acid concentrations was used, due to the problems concerning humic acid aggregation at high concentrations, and to detection limits at lower concentrations (especially after adsorption) (Palmer et al., 2002).

TiO_2 nanoparticles were dispersed into PPHA solution and shaken on a horizontal shaker for a time determined by the equilibrium experiment (See Appendix Time study). The unsorbed PPHA was separated from the sorbed by centrifugation at 7000 rpm for 30 minutes to precipitate and separate TiO_2 nanoparticles. Further it was measured with the Fluorescence Spectrometer, using an Excitation/Emission wavelength of 425/550 nm, corrected with the blank signal, and converted to mg C/L.

2.2.3. Irradiation Experiment

Samples were prepared containing 10 mg C/L PPHA at pH 4.5 and Titanium dioxide concentrations of 50, 100 and 200 mg/L. Before irradiation started, samples were kept shaking in the dark for 30 min to reach sorption equilibrium. After this time, samples were irradiated using the ATLAS Suntests CPS+. The radiation source was a 1.5 kW Xenon lamp. The spectrum of the solar UV simulator contained relatively small portions of visible light compared to real sunlight (300 nm < λ < 400 nm), the light intensity striking on the surface of the reaction solution was 65 W/m^2.

5 ml of sample were collected every 0, 5, 10, 15, 30, 60, 90 and 120 minutes, centrifuged (7000 rpm) and passed through a 0.02 µm syringe filter. The complete separation of nano-TiO_2 is the key to obtain clean signals, since it was found that small amounts of TiO_2, remaining in the solution, affect the spectrum of humic acids (Data not shown). Samples were characterized first with UV/Vis Spectrometer and Spectrofluorometer, and then samples were diluted 1:5 with the mobile phase in order to be characterized by HPSEC.

2.3. Samples characterization

2.3.1. UV-Vis Adsorbance

The UV-Vis absorbance of PPHA in the range λ=200 nm to 700 nm was measured with the PerkinElmer Lambda 35 UV/Vis Spectrophometer. UV-Vis parameters were calculated as indicative of photocatalytic degradation efficiency (Valencia et al., 2013):

A_{260}: Any wavelength from 220 to 280 nm has been considered to be most appropriate for NOM measurements, and they are believed to identify different chromophores (Matilainen et al., 2011). 260 nm was chosen for comparison with other measurements. The decrease in the signal implies loss of aromaticity.

A_{253}/A_{203}: The changes of A_{253}/A_{203} ratio of HS suggest that aromatic rings substituted with various functional groups in the HS molecules are structurally altered by physicochemical water treatment. The A_{253}/A_{203} ratio is low for unsubstituted aromatic ring structures and increases for the aromatic rings highly substituted with hydroxyl, carbonyl, ester and carboxylic groups.

These functional groups are also considered to participate preferentially in the reactions generating DBPs. A_{253}/A_{203} was as effective as UV_{254} (UV absorbance at 254 nm) to predict the formation potential of DBPs. Therefore, A_{253}/A_{203} ratio is a good indicator of the tendency for the DBPs (Kim and Yu, 2007).

A_{250}/A_{365}: Has been reported to correlate molecular size and aromaticity. The ratio increases as the aromaticity and molecular size decreases (Uyguner and Bekbolet, 2005b).

A_{254}/Color$_{436}$: Indicates the relative number of UV absorbing functional groups to color-absorbing groups in a molecule. Larger values of this ratio indicate higher rates of the removal of color forming moieties. In addition, it represents an alternative indicative parameter for the determination of photocatalytic degradation activity (Uyguner and Bekbolet, 2005a, b).

Color$_{465}$/Color$_{665}$: Smaller values are related to decreased aromaticity and to a degree of aggregation of organic solutes (Valencia et al., 2013).

2.3.2. Fluorescence

The excitation-emission matrix (EEM) fluorescence of each sample was obtained using the Fluoromax-4 Spectrofluorometer (HORIBA Scientific). EEMs were recorded in the excitation wavelength range of λ_{ex}=200-700 nm with a step width of 5 nm and in the emission wavelength of λ_{em}=250-750 nm with a step width of 5 nm.

2.3.3. HPSEC-UV/Vis-Fluorescence-ICP-MS

An HPLC system equipped with a micro-vacuum degasser was used with a 300 x 8 mm Toyopearl HW 55S (Grace Davison Discovery Sciences, Alltech Grom GmbH, Rottenburg-Hailfingen, Germany). Detection of particles was performed with the Agilent 1200 UV-DAD detector, Agilent 1200 3D-fluorescence detector, and ICP-MS Triple Quad (Agilent 8800).

The mobile phase consisted of a 25 mM solution of Ammonium Carbonate containing Ammonium carbamate ($CH_6N_2O_2.CH_5NO_3$, 1:1, Merck EMSURE®). The SEC column was followed by a DAD tuned to λ=260 nm, and a fluorescence detector with λ_{ex}=250 nm and λ_{em}=410 nm. An ICP-MS Triple Quad (Agilent 8800) was coupled to the outlet of the fluorescence detector. This set-up allows the elemental composition to be determined as a function of colloid size (Neubauer et al., 2013). Al, Fe, As, Pb, Cu, Ni and Mn were analyzed.

A flow rate of 0.3 mL/min was used. 200 µl was the volume of sample injected, and 25 µl was the volume for the molecular weight standards. The column was calibrated with molecular weight standards of 1100, 3610, 6780, 10600, 16800 and 32900 g/mol. The standards were prepared from polystyrene sulfonate sodium salt (PSS, Polymer Standards Service GmbH, Mainz, Germany) at 0.1 g/L concentration in the mobile phase.

3. Results and discussion

3.1. Photocatalytic activity

The photocatalytic activity of TiO_2 was evaluated by using 50, 100 and 200 mg/L of TiO_2 for complete degradation of 1.5 ppm aqueous MB solution on illumination with 1.5 kW Xenon lamp. The results of photocatalytic activity of TiO_2 samples towards the degradation of MB are shown in Figure 2.

The graph depicts the relative concentration of MB in solution (C/C_o) with irradiation time, and shows that there was no difference in the degradation of MB with variation of TiO_2 concentration. The adsorption of MB onto TiO_2 in the dark was very small, as confirmed also by Toyoda et al. (2004), showing that the observed decrease in absorbance and concentration in the solution was due to the decomposition of MB by the photocatalytic activity of TiO_2.

Tryba et al. (2007) concluded that the MB decomposition on TiO_2 samples was not only determined by the reaction with $OH^{\cdot}$, but also by the direct reaction of adsorbed MB molecules with photogenerated holes. We can conclude from this experiment that TiO_2 is producing radicals under the study conditions, which could cause molecular changes, and possible degradation, in the PPHA in solution and adsorbed.

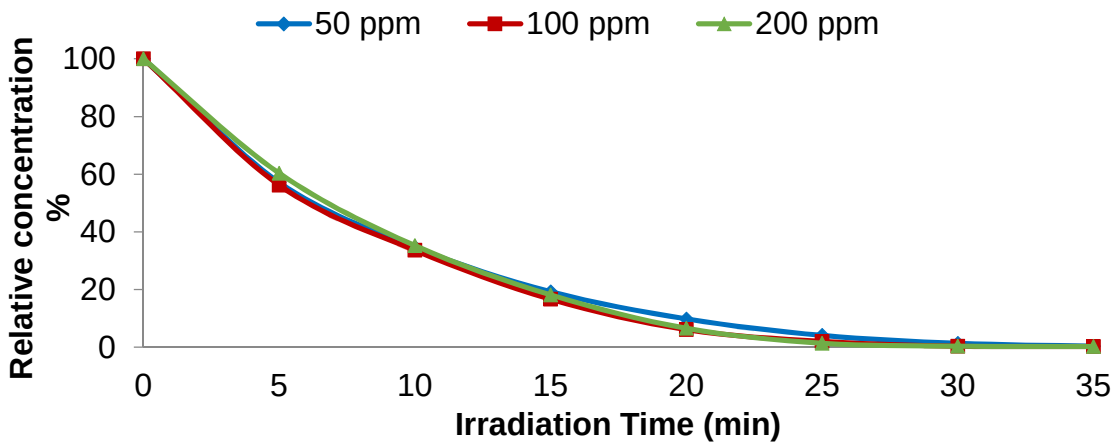

Figure 2 Photocatalytic activity of TiO_2 at different concentrations; Y axis is the relative concentration of Methylene Blue in solution.

3.2. Adsorption Isotherm

Humic acid adsorption onto TiO_2 is pH-dependent and mainly induced by electrostatic attraction and ligand exchange between HA and nano-oxides surfaces (Valencia et al., 2012). Adsorption of PPHA was measured after 30 minutes of contact time, using different dosages of TiO_2. As TiO_2 concentration increased, a greater surface area and a greater number of biding sites were available for the constant amount of PPHA, which resulted in the increasing PPHA removal with the increasing TiO_2 concentration (Figure 3).

The adsorption of humic acids on a solid surface is a complex process that depends on the chemical nature of the TiO_2 surface and the PPHA as well as the solution properties. The chemical behavior of humic acid is controlled by two functional groups: the carboxyl and the phenolic-OH groups (Liu et al., 2014). At pH 4.5 the carboxyl group has its protons dissociated, and the humic molecules are negatively charged, while TiO_2 is more positively charged, benefiting adsorption. In acidic conditions, humic acids can be absorbed on TiO_2 surface and react with $OH^{\cdot}$ on TiO_2 surface, which also prevent $OH^{\cdot}$ from diffusing to the solution (Xiaoju et al., 2012).

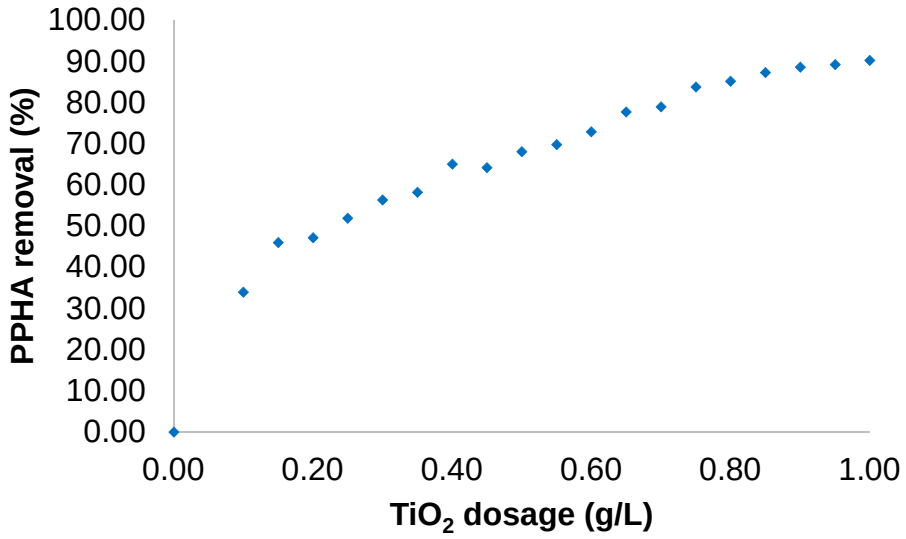

Figure 3 Effect of TiO_2 concentration on the adsorption of PPHA. Adsorption conditions: pH 4.5, temperature 25 °C, initial DOC content=20 mg/L.

The equilibrium adsorption of PPHA onto TiO_2 nanoparticles at pH 4.5 is shown in Figure 4. Isotherms for the adsorption of PPHA onto TiO_2 were constructed by plotting the equilibrium concentration (C_e) against the amount of humic acid adsorbed per gram of titanium dioxide (q_e).

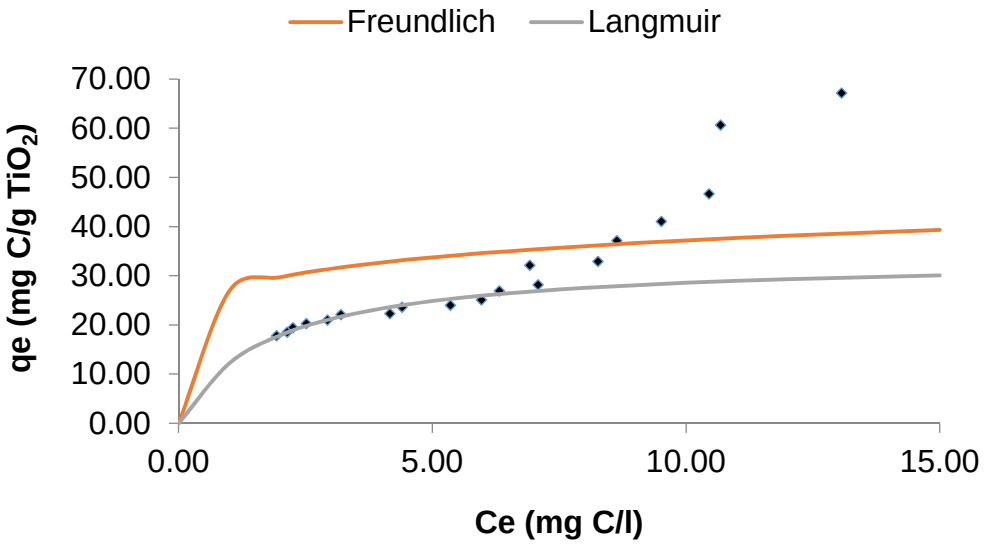

Figure 4 Adsorption isotherms of PPHA at pH 4.5 by nano-TiO_2: points refer to experimental data and lines refer to fitting of models.

The isotherm observed in the first part of the graph, ρ(TiO_2) from 1 g/L to 0.5 g/L, can be classified as an L-shape without strict plateau, which suggests a progressive saturation of the solid, but the solid does not show clearly a limited sorption capacity. (Limousin et al., 2007).

However, the second part of the graph, where the concentrations of TiO_2 are lower (0.1-0.35 g/L), did not adjust to the models, and resembles more an "S" isotherm with a sigmoidal curve that has a point of inflection. This type of isotherm is always the result of at least two opposite mechanisms. Non-polar organic compounds are a typical case: they have a low affinity with clays. But as soon as a clay surface is covered by these compounds, other organic molecules are adsorbed more. This phenomenon is called ''cooperative adsorption'' and is also observed for surfactants. The presence of a soluble ligand can also provide a sigmoidal isotherm for metallic species. At low metal concentrations,

the adsorption is limited by the presence of the ligand. The ligand must be saturated and then the adsorption occurs normally. The point of inflection illustrates the concentration for which the adsorption overcomes the complexation (Limousin et al., 2007).

The adsorption of PPHA onto TiO_2 increased with the increased initial TiO_2 concentrations. The Langmuir and Freundlich models were fitted to the isotherm data (See Table Appendix Table 5). The constants in the Langmuir isotherm were determined by plotting C_e/q_e versus C_e and making use of the Langmuir equation rewritten as (See Appendix Figure 31):

$$\frac{C_e}{q_e} = \frac{1}{K_L Q_{max}} + \frac{C_e}{Q_{max}}$$

where Q_{max} and K_L are the Langmuir constants representing the maximum adsorption capacity for the solid phase and the Langmuir constant related to the binding strength, respectively.

The Freundlich model is an exponential equation expressed was:

$$q_e = K_F C_e^{1/n}$$

where K_F represents the extent of adsorption and is the amount of HA adsorbed per unit mass of adsorbent, and n is the heterogeneity factor related to the intensity of adsorption which varies with the heterogeneity of this material. The values of K_F and 1/n were determined from the slope and intercept of the $\ln(q_e)$ versus $\ln(C_e)$ plots (See Appendix Figure 32).

The fitting results are presented in Table 2:

Table 2 Parameters of the Langmuir and Freundlich adsorption isotherm for PPHA/TiO_2

Model	Parameters	Value
Langmuir	q_{max} (mg/g)	33.56
	K_L (l/mg)	0.57
	R^2	0.9841
Freundlich	K_F (mg/g)	26.94
	1/n	0.1397
	R^2	0.9775

Langmuir isotherm presented a best fit. In its formulation, this empirical model assumes monolayer adsorption (the adsorbed layer is one molecule in thickness), with adsorption can only occur at a finite (fixed) number of definite localized sites, which are identical and equivalent, with no lateral interaction and steric hindrance between the adsorbed molecules, even on adjacent sites.

In its derivation, Langmuir isotherm refers to homogeneous adsorption, which each molecule possess constant enthalpies and sorption activation energy (all sites possess equal affinity for the adsorbate), with no transmigration of the adsorbate in the plane of the surface (Foo and Hameed, 2010).

Since HA is known to consist of a complex mixture, adsorption equations which describe the adsorption of a single adsorbate, such as the Langmuir, may not be appropriate for interpretation of data (Erhayem and Sohn, 2014).

3.3. Irradiation

3.3.1. UV/Vis Absorbance

UV-Vis spectra of humic acids is broad, featureless and monotonously decreasing with increasing wavelength (Uyguner & Bekbolet, 2005a). Figure 5 shows UV-Vis absorption spectra of PPHA during photocatalytic degradation as a function of irradiation time. The initial state of PPHA is represented by the black line.

The photocatalytic decomposition of PPHA was performed after its adsorption on the TiO_2 surface, therefore, to evaluate the photocatalytic activity of the samples, the concentration of PPHA after adsorption was taken as an initial PPHA concentration. After 30 minutes of equilibration, the adsorption was for (a) 15%, making the spectrum decrease steadily with increasing irradiation time. For (b) and (c), around 90% of the sample was adsorbed by TiO_2.

The spectrum showed a small decreased in absorbance, and it is thought that the processes of desorption and degradation are occurring at the same time. At 120 minutes, the three experiments show almost the same pattern, indicating that complete mineralization could not be achieved.

Matilainen and Sillanpää (2010) concluded that a drop in UV_{254} values suggests that the chromophores in the NOM macro-molecules, which consist mainly of HMW aromatic rings, are rapidly broken down into LMW by-products, with no UV absorbance. These by-products are thus less susceptible to attacks by $OH^{\cdot}$ and therefore not mineralized completely.

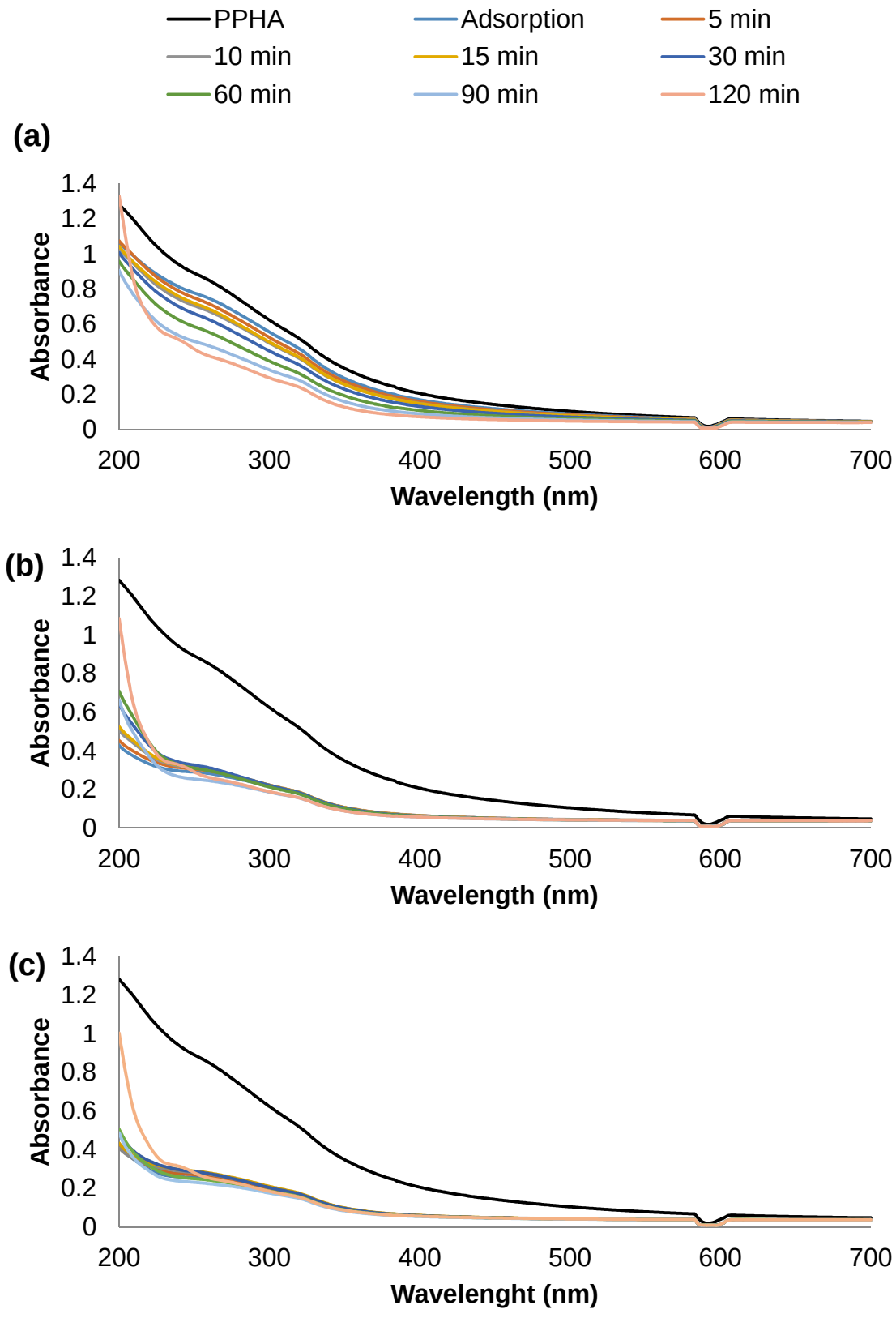

Figure 5 UV-Vis absorption of PPHA during photocatalytic degradation. HA Initial concentration ≈ 10 mg/L; (a) TiO_2 = 50 mg/L; (b) TiO_2 = 100 mg/L; and (c) TiO_2 = 200 mg/L

The concentration of PPHA remaining in the samples was calculated from the calibration curve at 260 nm. Figure 6 shows how the behavior of degradation is influenced by the load of TiO_2.

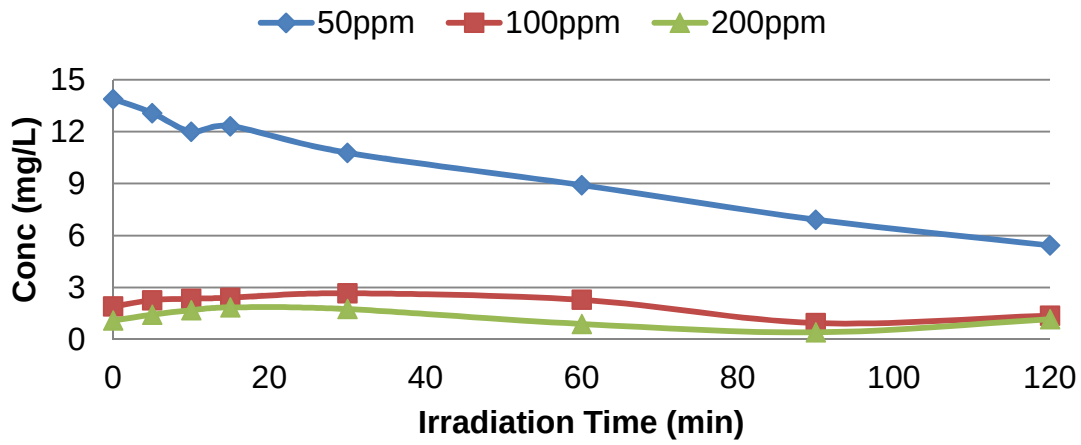

Figure 6 Residual concentration changes of PPHA over time

The relative concentration in solution was calculated to see the percentage of degradation (Fig. 7). While the sample with lower TiO_2 concentration showed a steady decrease, the higher concentration showed patterns of increase and decrease, again pointing at desorption and degradation processes occurring simultaneously.

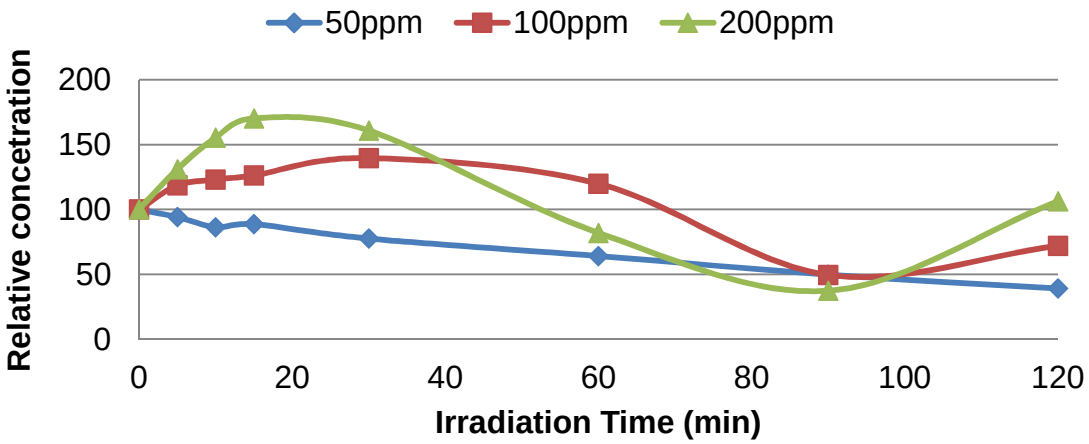

Figure 7 Relative concentration of PPHA in solution with different TiO_2 concentration.

Figure 8, 9, 10 and 11 show the UV absorption ratios for the remaining PPHA after UV/TiO_2 treatment. The A_{253}/A_{203} ratio decreased from 0.70 to 0.38, 0.30 and 0.31 with 50, 100 and 200 ppm of TiO_2, respectively, after 120 minutes of irradiation, decreasing the potential of formation of DBPs and the aromaticity of the molecule.

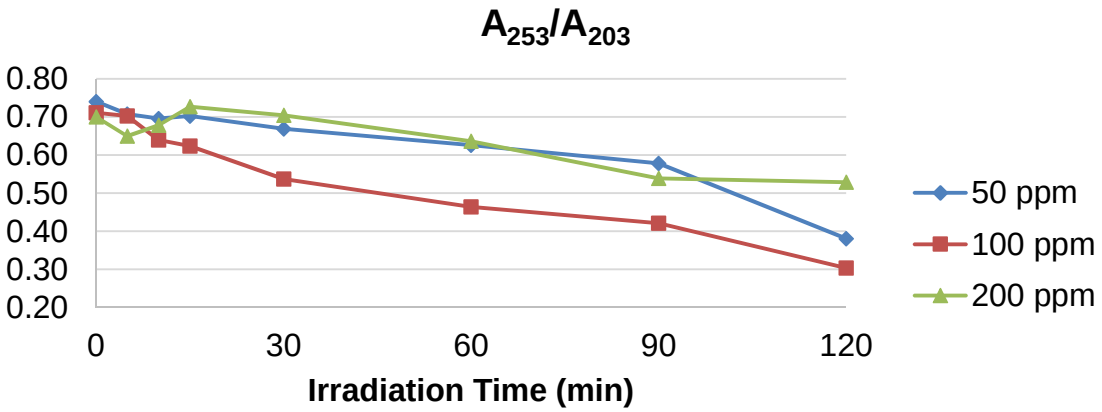

Figure 8 Spectroscopic ratio A_{253}/A_{254} of the remaining PPHA after UV/TiO_2 treatment with different TiO_2 concentrations at pH 4.5

The A_{250}/A_{365} increased from 3.04 to 4.52, 3.99 and 3.92 with 50, 100 and 200 ppm of TiO_2, respectively, after 120 minutes of irradiation, showing that molecular size and aromaticity were decreasing.

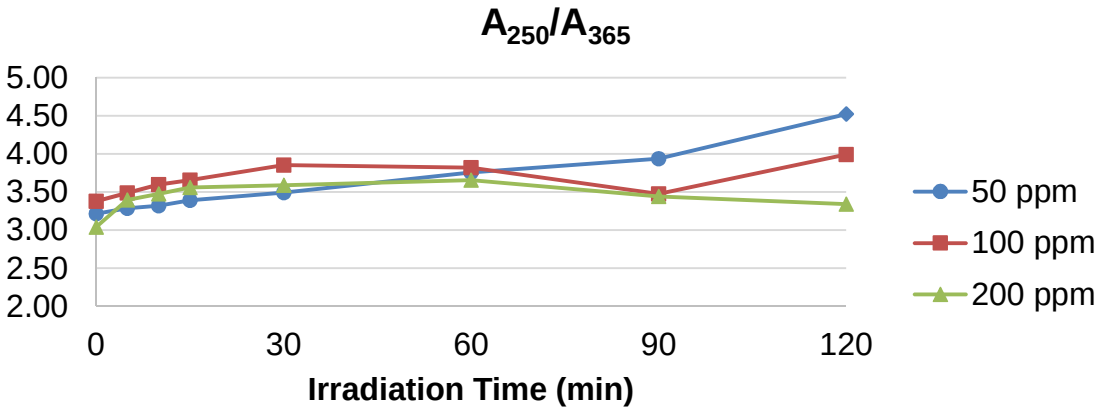

Figure 9 Spectroscopic ratio A_{250}/A_{365} of the remaining PPHA after UV/TiO_2 treatment with different TiO_2 concentrations at pH 4.5

In contrast, $A_{254}/Color_{436}$ behaved differently with TiO_2 concentrations. Values in the range of 4-11 have been reported for terrestrial dissolved organic matter which has a greater organic matter content associated with the presence of tannin like or humic like substances derived from plants and soil organic matter (Uyguner and Bekbolet, 2005b).

With 50 ppm TiO_2, the ratio increased from 5.60 to 7.31, indicating removal of color forming moieties. However, for 100 and 200 ppm, the ratio did not experience changes, which could be due to the larger amount adsorbed after 30 minutes of equilibration, or due to adsorption-desorption phenomena happening during irradiation.

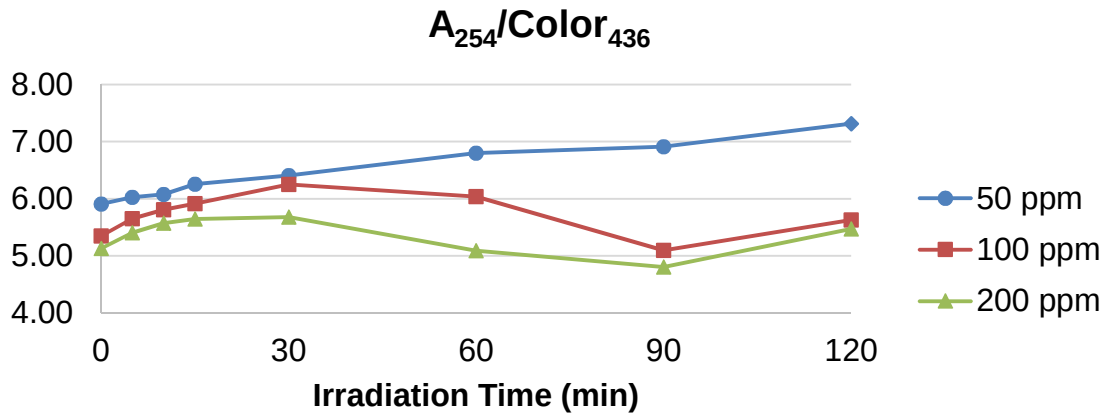

Figure 10 Spectroscopic ratio $A_{254}/Color_{436}$ of the remaining PPHA after UV/TiO_2 treatment with different TiO_2 concentrations at pH 4.5

$Color_{465}/Color_{665}$ decreased from 2.53 to 1.32, 1.21 and 1.20 with 50, 100 and 200 ppm of TiO_2, respectively, after 120 minutes of irradiation this confirmed the decrease in aromaticity and degree of aggregation of the organic molecule. Values of $Color_{465}/Color_{665}$ are usually <5.0 for HAs (Uyguner and Bekbolet, 2005b),

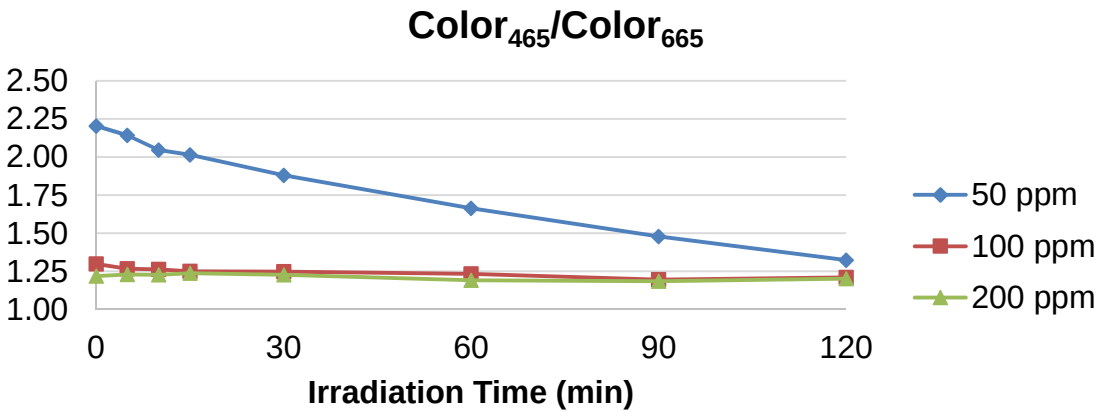

Figure 11 Spectroscopic ratio $Color_{465}/Color_{665}$ of the remaining PPHA after UV/TiO_2 treatment with different TiO_2 concentrations at pH 4.5

3.3.2. Fluorescence

Figures 12, 13 and 14 show the EEM contour plots of PPHA with different TiO_2 concentrations, after irradiation. Photocatalysis led to an almost continuous reduction of the fluorescence intensity and changes in the shape of the EEM.

Changes in the spectrum were visible for the three concentrations of TiO_2 in different degrees, but with TiO_2 = 200 mg/L the decrease of fluorescence intensity of PPHA was higher. In all cases, the photocatalytic degradation shifted the fluorescence maxima towards shorter wavelengths.

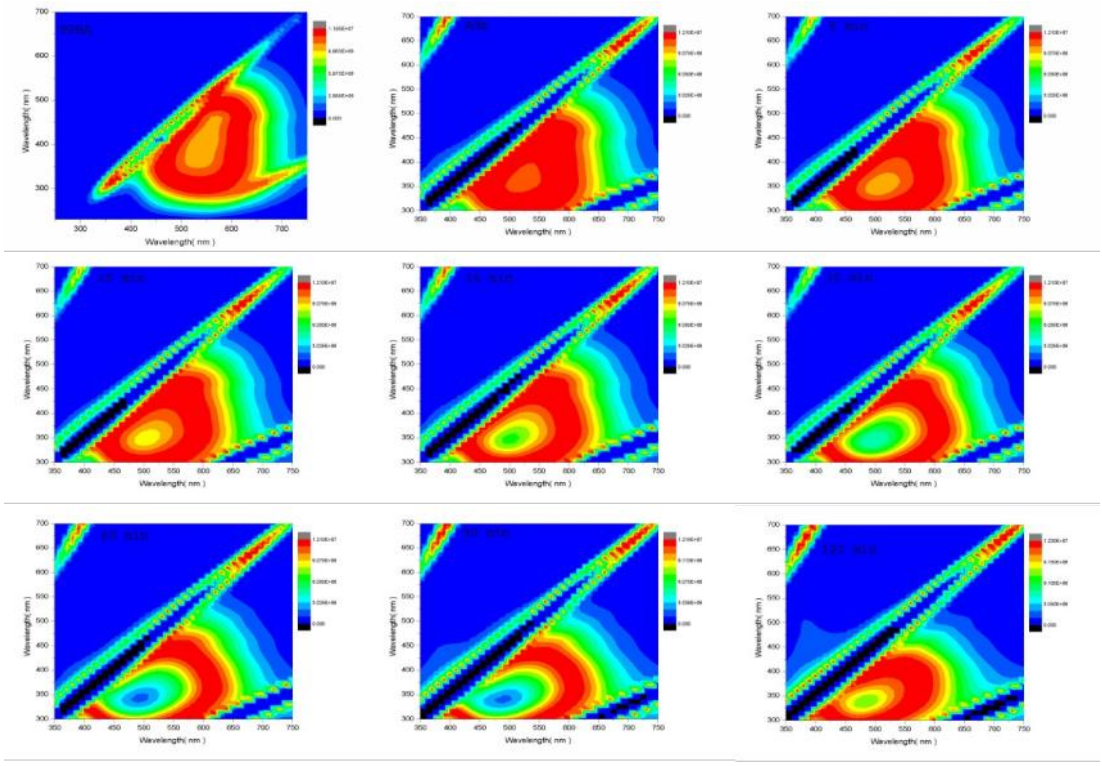

Figure 12 EEM fluorescence diagrams for the remaining PPHA after UV/TiO_2 treatment as a function of irradiation time: HA ≈ 10 mg/L, TiO_2 = 50 mg/L.

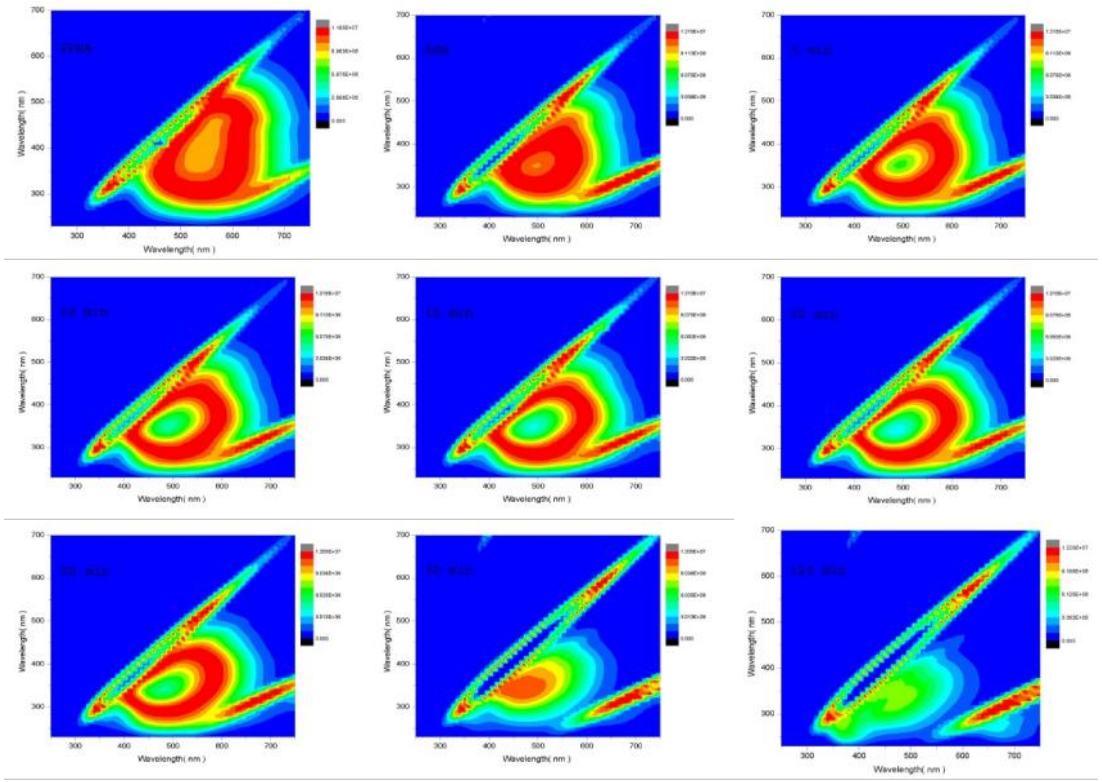

Figure 13 EEM fluorescence diagrams for the remaining PPHA after UV/TiO_2 treatment as a function of irradiation time: HA ≈ 10 mg/L, TiO_2 = 100 mg/L.

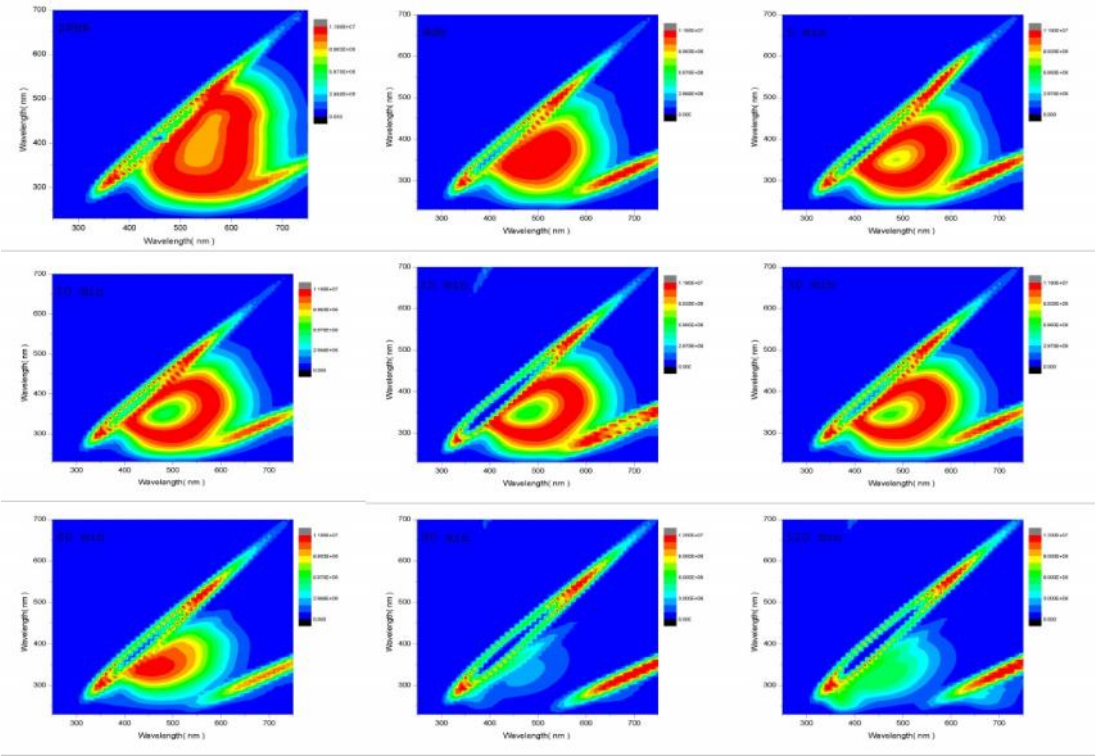

Figure 14 EEM fluorescence diagrams for the remaining PPHA after UV/TiO_2 treatment as a function of irradiation time: HA ≈ 10 mg/L, TiO_2 = 200 mg/L.

Valencia et al. 2013 concluded that the decreased fluorescence intensity in the EEM plots of Aldrich HA was due to preferential photocatalytic degradation of higher molecular weight fractions. In our experiments, this preferential degradation also led to the formation of lower molecular weight fractions, which was supported by the other analysis.

A strong linear correlation between Fluorescence intensity and DOC has been observed by Valencia et al. 2013 and Bieroza et al. 2009. As a result, the decrease in fluorescence intensity could be used as an indicator of DOC removal efficiency.

3.3.3. HPSEC-UV--Vis-Fluorescence

Figure 15 shows the PPHA standards measured with both detectors. The humic acid eluted from the HPSEC column as broad, unimodal distributions with subtle shoulders and small sub-peaks. The inability of HA to be separated into discrete components, defined by distinct MW fractions, reflects the fact that they are complex mixtures of high to low molecular weight species, that are difficult to resolve chromatographically (O'Loughlin and Chin, 2001).

An analysis of the SEC chromatograms showed that slight shifts toward lower retention times (i.e., higher MW values) were responsible for the apparent increase in MW as PPHA concentrations increased. The maximum peak of PPHA eluted at 31.55-31.13 min for DAD, and at 34.54-34.31 min for FLD.

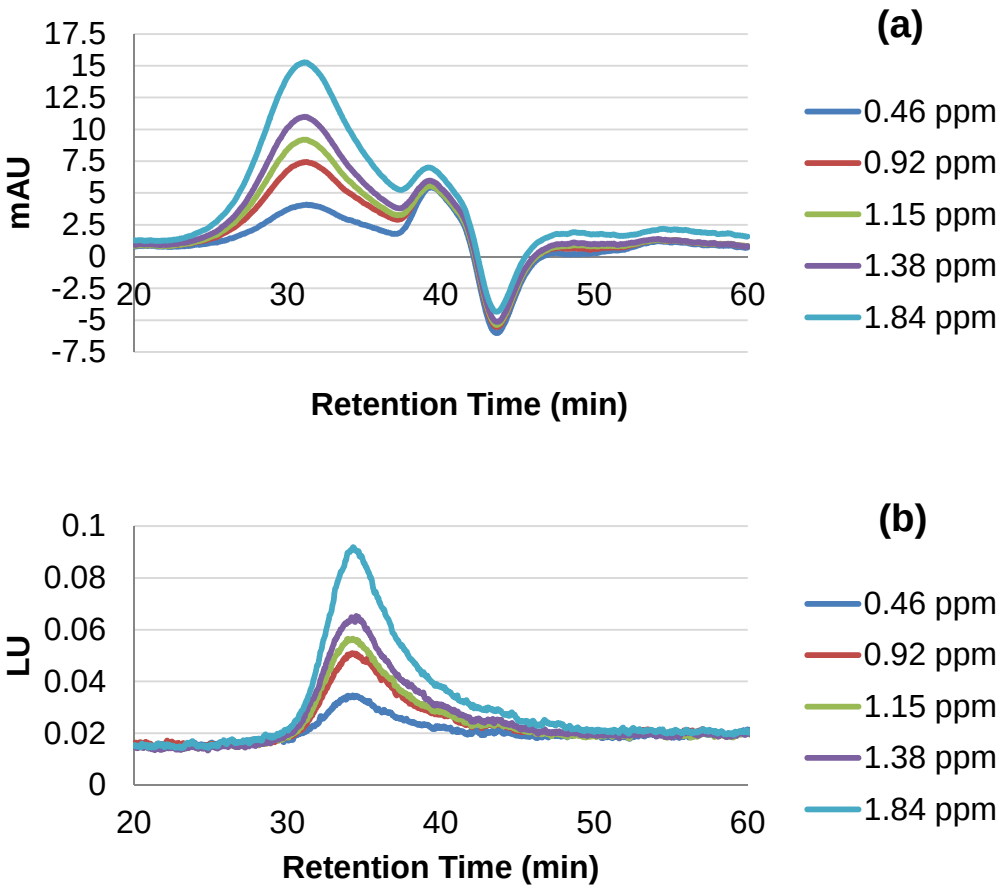

Figure 15 PPHA standards SEC chromatograms with (a) UV_{260} and (b) FLD λ_{ex}=250 nm, λ_{em}=410 nm

Although, no concentrations were calculated from these calibration curves, it was important to check the linear response of the detectors. The R-square values, calculated with the area below the peak and the standard concentration, were R^2=0.9764 and R^2=0.9566 for DAD and FLD, respectively.

Figure 16 shows the chromatograms for the Molecular weight standards measured with both detectors. All molecular mass standards were injected at the same concentration. However, the responses of the detectors were not equal. Smaller particles have less UV-Vis absorbance, but the fluorescence does not seem to be related to the particle size. Calibration curves were constructed by linear regression of logMW-t_R, and the R^2 were 0.847 for DAD, and 0.9941 for FLD.

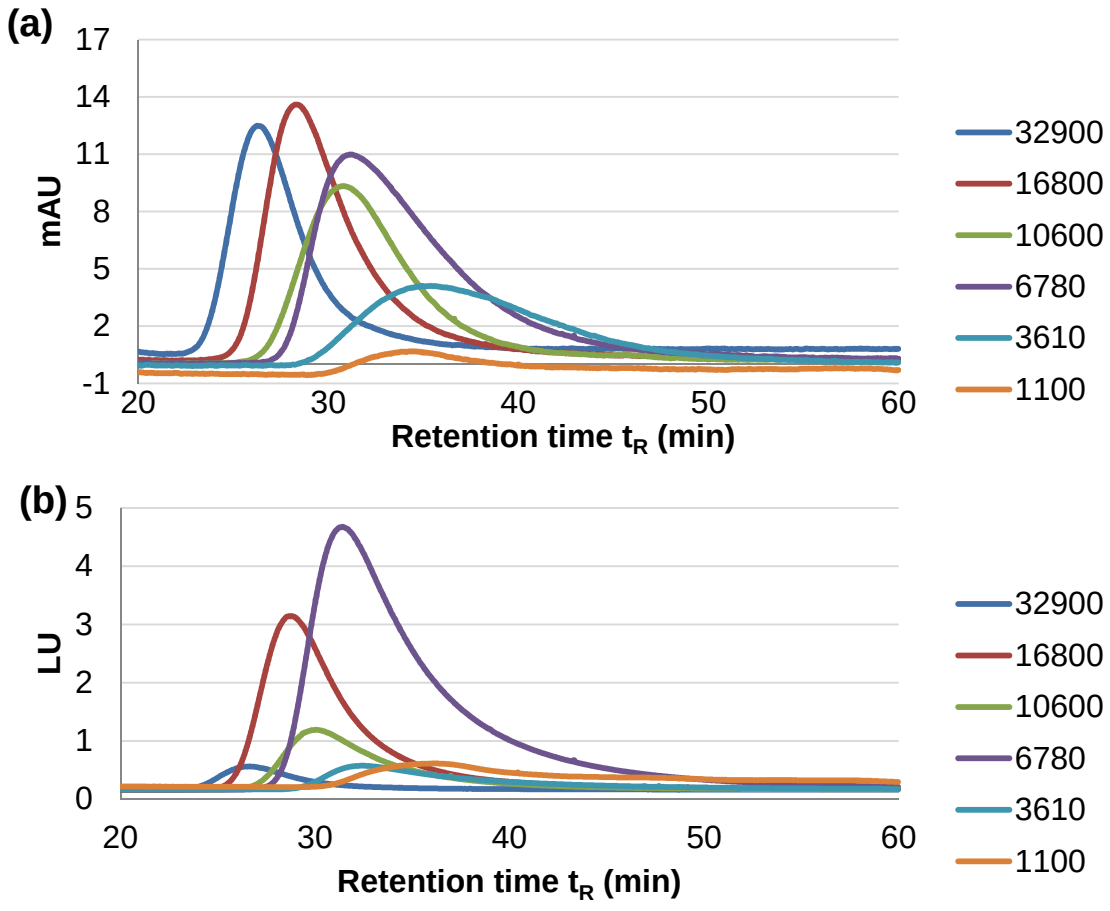

Figure 16 Chromatograms for Molecular weight standards measured with (a) DAD UV_{260} and (b) FLD λ_{ex}=250 nm, λ_{em}=410 nm

Figure 17 shows the changes in retention time of the maximum peak of PPHA with irradiation time, measured with DAD. The signals of water blanks have been subtracted from the samples. Axes differ in the three graphs to better illustrate.

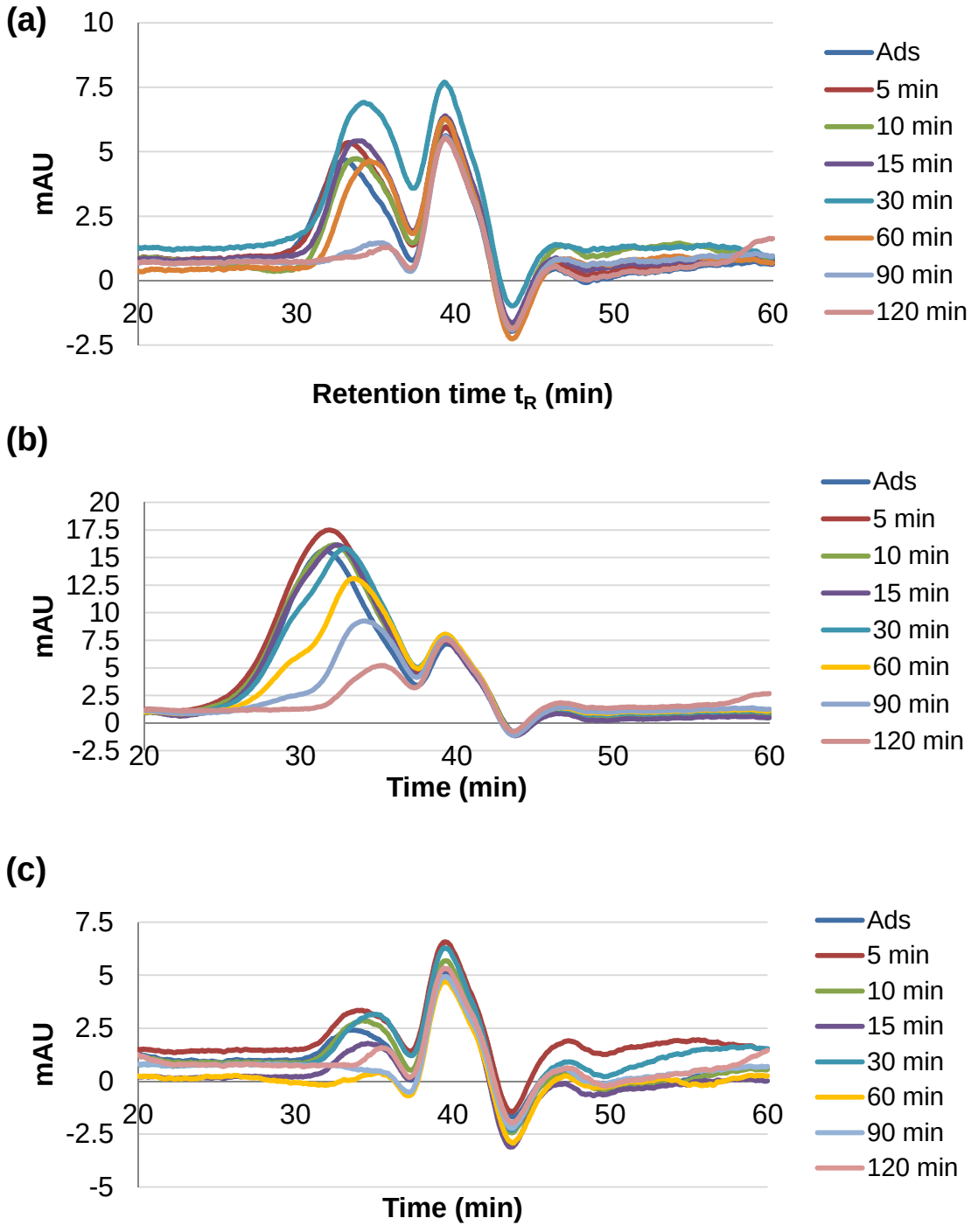

Figure 17 HP-SEC chromatograms of HA measured with UV_{260} absorption after photocatalytic degradation; (a) TiO_2 = 50 mg/L; (b) TiO_2 = 100 mg/L; and (c) TiO_2 = 200 mg/L

The adsorption of PPHA onto TiO_2 after 30 minutes of equilibration was very marked (Ads), but it was not directly proportional to the TiO_2 concentration. With TiO_2 = 50 mg/L, PPHA Ads eluted at 33.14 min and, after 120 min of irradiation, the maximum peak shifted to 37.07 min. With TiO_2 = 100 mg/L, the peak shifted from t_R = 31.54 min to 35.23 min. For TiO_2 = 200 mg/L, the peak started at 34.04 min, then it disappeared after 60 minutes of irradiation, and appears after 120 minutes with an t_R=35.69min.

Figure 18 shows the changes in the retention time of the characteristic peak of PPHA after irradiation, measured with FLD. Water blank have been subtracted from the samples, and the axes differ in the three graphics to better illustrate.

With TiO_2=50 mg/L, after adsorption PPHA eluted at 34.54 min, after 90 min of irradiation the peak shifted to 36.84 min, and there was no visible peak after 120 min With TiO_2 = 100 mg/L the peak shifted from t_R = 34.50 min to 35.34 min. For higher TiO_2 concentration the peak started at 34.85 min after 30 minutes of irradiation it shifted to 35.21min, and it disappear.

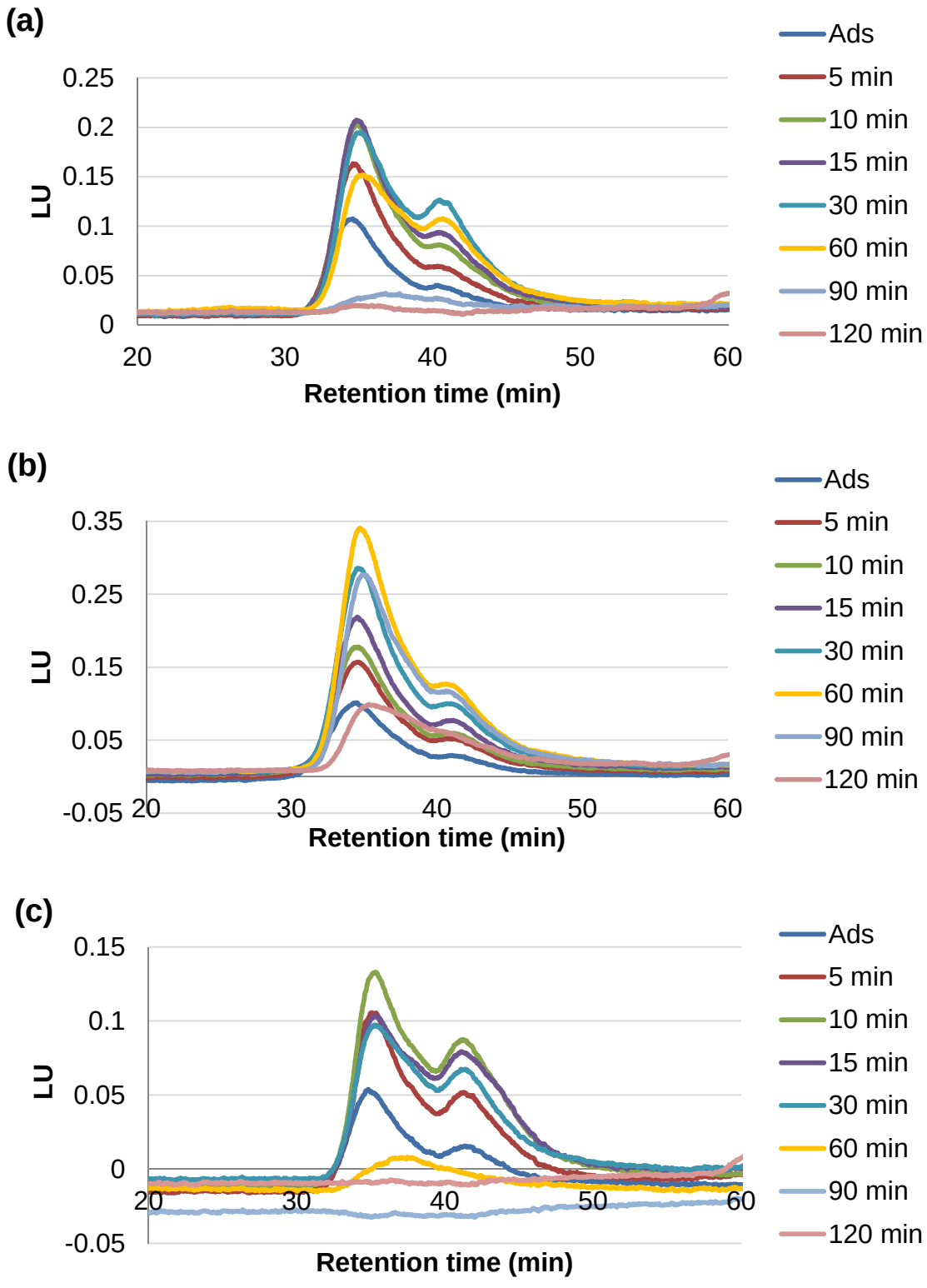

Figure 18 HP-SEC chromatograms of PPHA measured with FLD at different irradiation times of the photocatalytic degradation; (a) TiO_2 = 50 mg/L; (b) TiO_2 = 100 mg/L; and (c) TiO_2 = 200 mg/L

The degradation process was characterized by the growth of the smaller fractions at the expense of the larger fraction. According to Tercero et al. (2009), this degradation sequence does not depend on either the high or low NOM adsorption or the preferential adsorption of the fraction with the higher molecular weight in the dark. In Figures 19 and 20 it is possible to see how different the adsorption in the dark was, and how it changed the original PPHA spectrum.

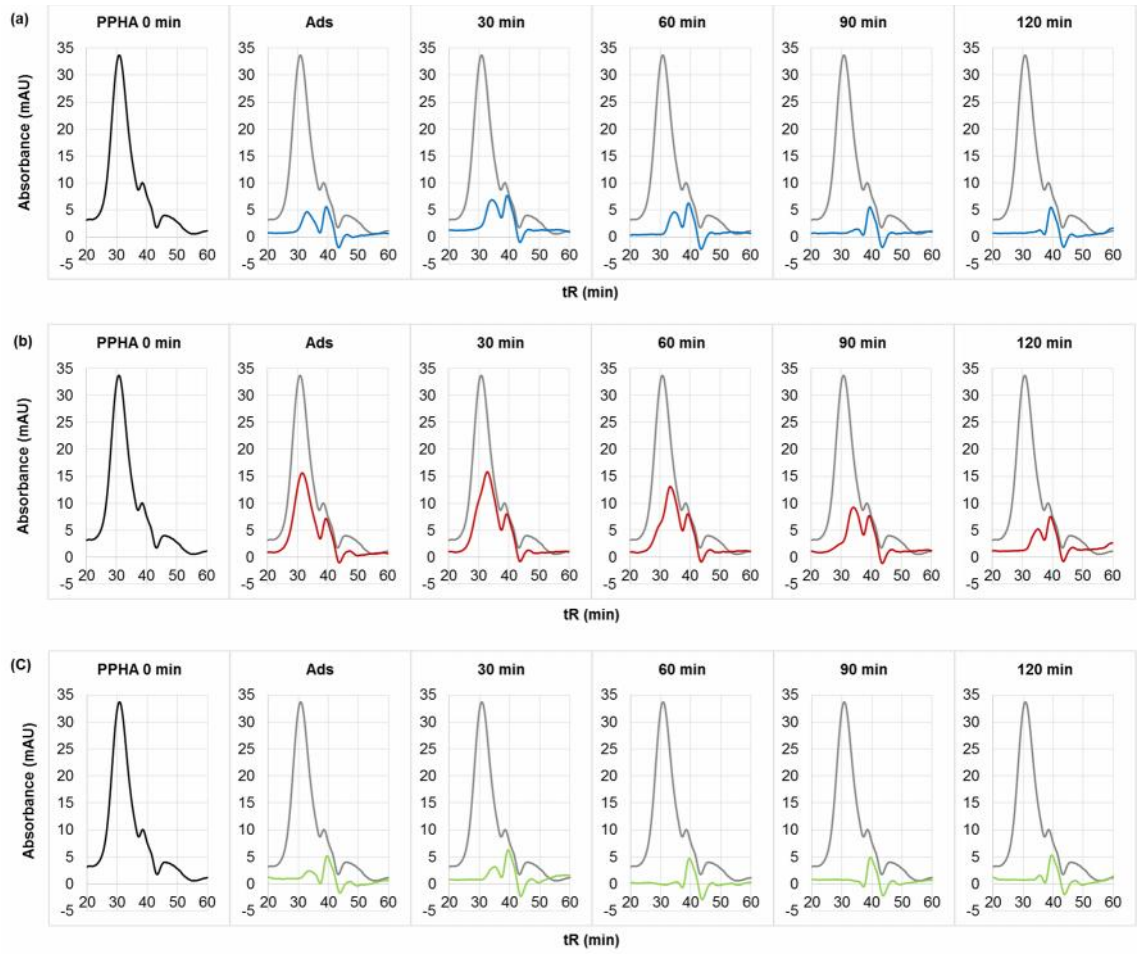

Figure 19 SEC-UV_{260} chromatograms of PPHA during UV/TiO_2 treatment at pH = 4.5 and their evolution, (a) TiO_2 = 50 mg/L; (b) TiO_2 = 100 mg/L; and (c) TiO_2 = 200 mg/L.

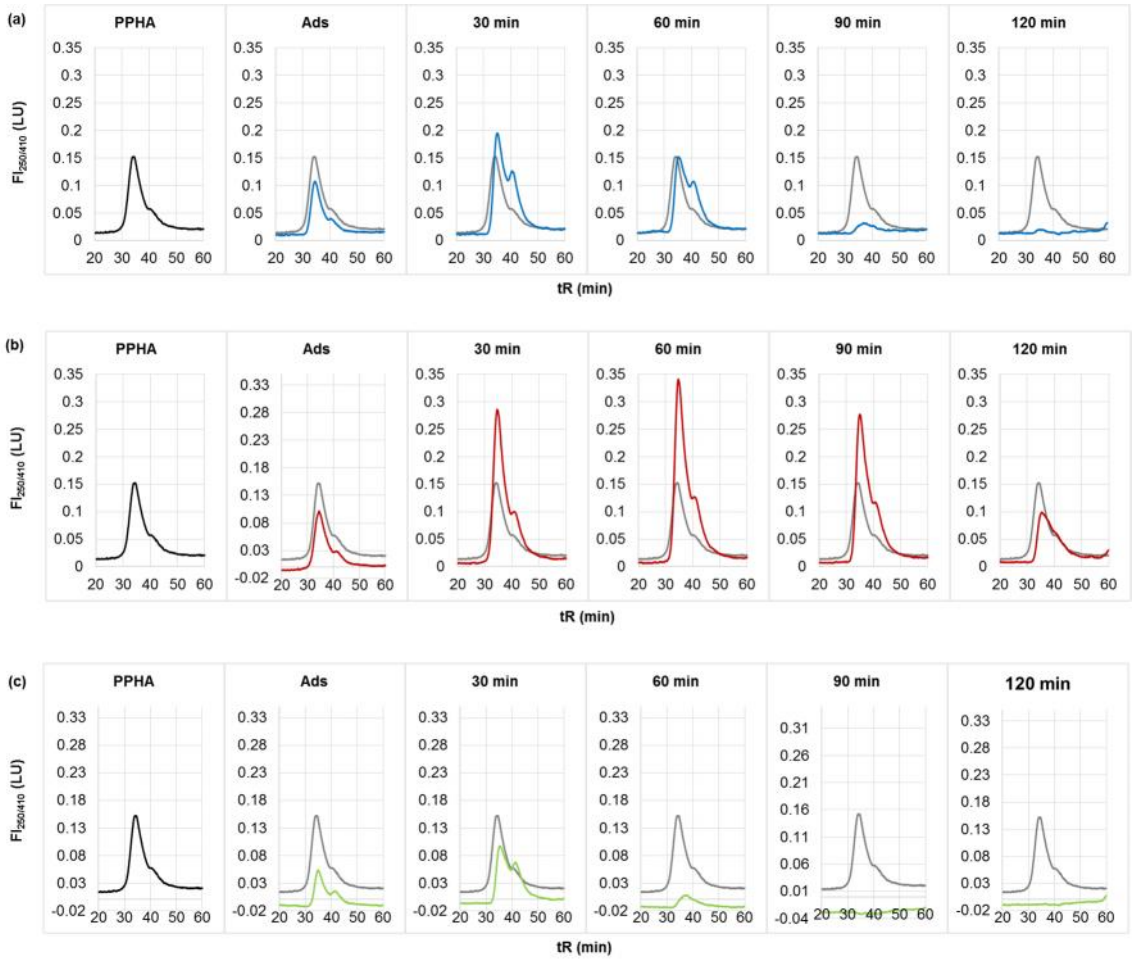

Figure 20 SEC-$Fl_{250/450}$ chromatograms of PPHA during UV/TiO_2 treatment at pH = 4.5 and their evolution, (a) TiO_2 = 50 mg/L; (b) TiO_2 = 100 mg/L; and (c) TiO_2 = 200 mg/L

Due to the tendency of higher molecular weight structures to be more aromatic, the reaction between $OH^{\cdot}$ and NOM depend on the molecular weight, resulting in larger number of reaction sites (Valencia et al., 2012). Table 3 shows the molecular weights of the remaining PPHA after irradiation. For DAD, the initial molecular weight distribution of PPHA showed the main peak at 8100 g/mol, and it degraded to LMW (~1500 g/mol). For FLD, the initial MW distribution of PPHA showed a main peak at 2400 g/mol, 4 times smaller than what was calculated by DAD.

Table 3 Calculated molecular weight of PPHA left in solution after irradiation

Sample		Retention time t_R DAD main peak	Molecular Weight (g/mol)	Retention time t_R FLD main peak	Molecular Weight (g/mol)
50 mg/L	0	33.14	3682.79	34.54	1856.33
	5	33.50	3273.49	34.80	1689.19
	10	33.83	2930.53	34.94	1603.86
	15	34.01	2766.05	34.85	1662.26
	30	34.32	2496.34	34.97	1586.76
	60	35.00	1997.10	35.22	1450.30
	90	35.58	1650.39	---	---
	120	37.07	1009.96	---	---
100 mg/L	0	31.54	6230.81	34.50	1883.38
	5	31.89	5554.89	34.58	1832.29
	10	32.18	5048.09	34.63	1796.22
	15	32.41	4672.71	34.53	1866.03
	30	32.84	4059.36	34.68	1763.42
	60	33.46	3307.34	34.70	1750.72
	90	34.09	2694.69	34.93	1611.77
	120	35.23	1852.43	35.34	1387.81
200 mg/L	0	34.04	2738.71	34.85	1661.53
	5	34.51	2348.28	35.04	1549.97
	10	34.68	2220.33	35.13	1497.36
	15	35.09	1936.05	35.36	1380.83
	30	35.08	1943.54	35.21	1455.98
	60	---	---	---	---
	90	---	---	---	---
	120	35.69	1589.53	---	---

Differences in the MW distribution calculated by DAD and FLD could be explained by the different response of the detectors to the molecular weight standards. As noted, FLD presented a better correlation for MW standards, but for PPHA standards both detectors have almost similar correlations. Obtaining appropriate standards for use in HPSEC measurements of NOM MW is difficult, because of the unique MW and charge distribution properties of humic materials (Zhou et al., 2000). Of the various standards available, PSS has charge density that is most similar to NOM, while structural similarity is debatable.

3.3.4. Apparent Molecular Weight distribution and binding of elements

Samples were analyzed again with the system HPSEC-UV/Vis-Fluorescence-ICP-MS. A multi-point calibration was performed prior to sample analysis. The results for the calibration are depicted in Figure 21. Even though 7 elements were analyzed, only those elements that were present in the samples are discussed, in order to simplify the results. All elements had very good correlations.

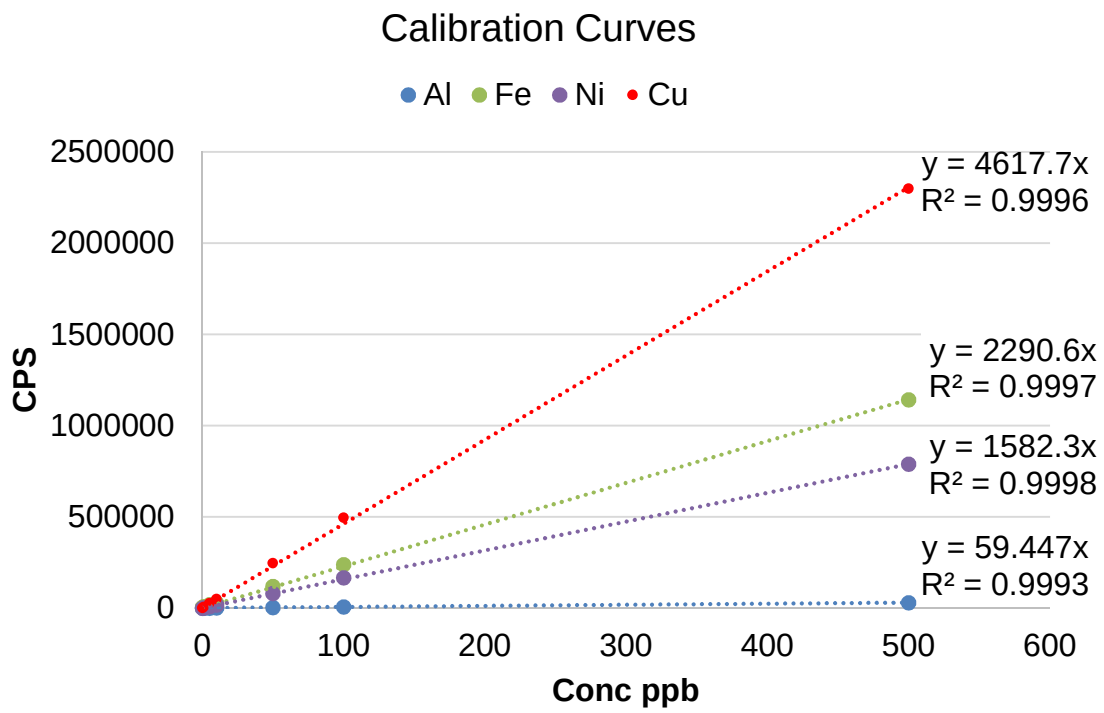

Figure 21 Multi-point calibration for the element analysis HPSEC-UV—Vis-Fluorescence-ICP—MS.

Figure 22, 23, 24 and 25 show the results for the three samples and their comparison with PPHA, at equilibration (0min) and after 120 min of UV-TiO_2 treatment. Samples with TiO_2 before irradiation presented baselines higher than in the PPHA blank. In all cases, there was a shift toward higher retention times, indicating an increased abundance of these elements within smaller fractions.

Aluminum (Fig. 22) showed no apparent peak in the samples before irradiation. After 120min of irradiation a peak at approx. 40 minutes appeared in the PPHA

blank, and the samples with 50 and 100 ppm of TiO_2. It is believed that Aluminum was released from the glassware (© 2015 Heraeus Quarzglas) with irradiation and that it was complexed by the small molecules of PPHA formed; once this small particles continue to be degraded (200 mg/L of TiO_2), the Al is released back into solution and disappears from the chromatogram.

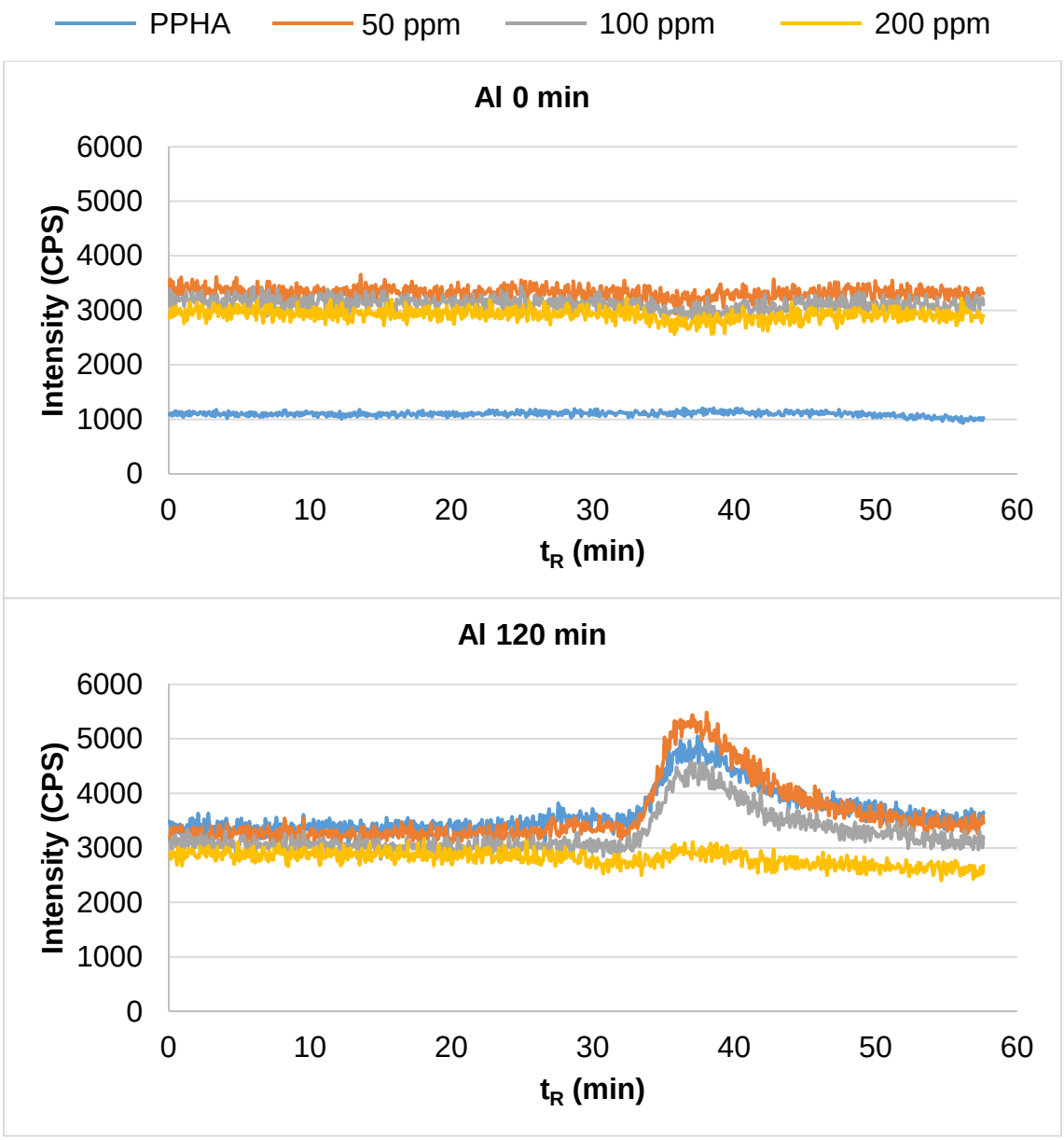

Figure 22 HPSEC – ICP-MS chromatograms for Aluminum, measured as UV-Vis signal at 260 nm.

Iron (Fig. 23) had almost the same initial signal, smaller for the 50 ppm sample. After 120 min, PPHA blank and 50 ppm sample signal increased, while 100 and 200 ppm were almost disappeared. The association with Iron could quench the fluorescence signal of the NOM (Neubauer et al., 2013), which is possibly why the response was smaller for FLD than for DAD.

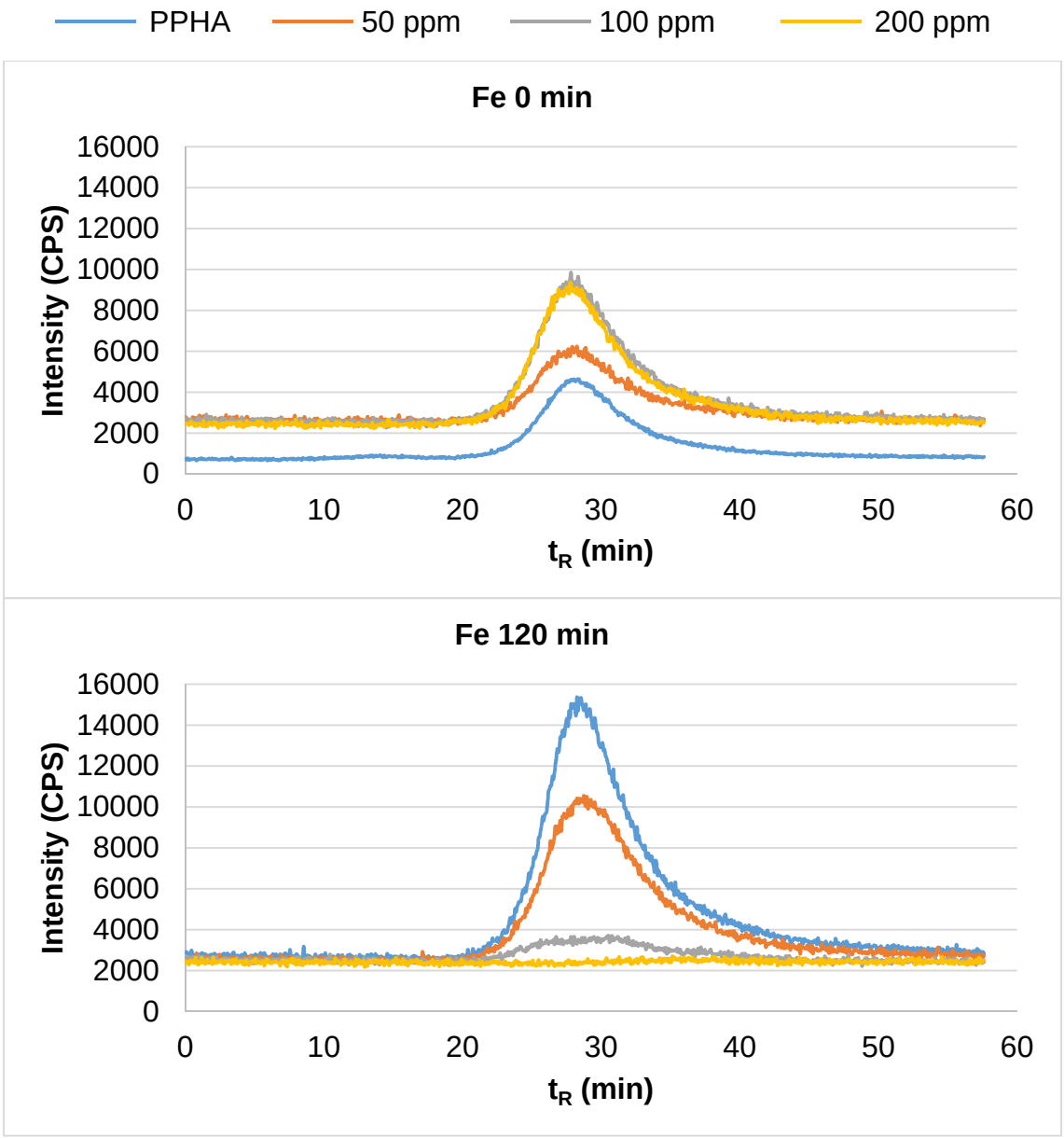

Figure 23 HPSEC – ICP-MS chromatograms for Iron, measured as UV-Vis signal at 260 nm.

Nickel (Fig. 24) and Copper (Fig. 25) had almost this same behavior, where signals of PPHA blank and 50 ppm increased after irradiation, and almost disappear for 100 and 200 ppm samples.

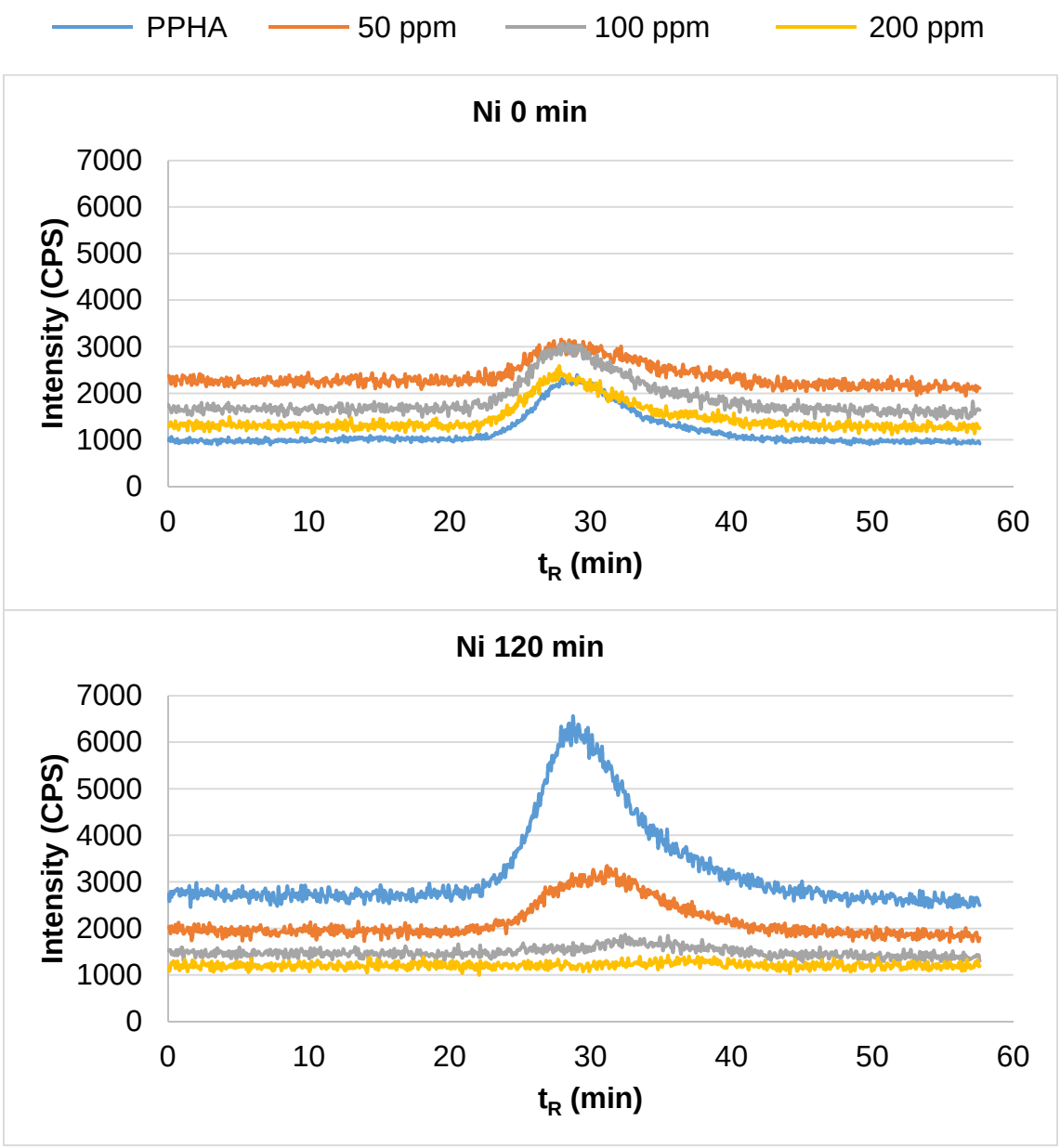

Figure 24 HPSEC – ICP-MS chromatograms for Niquel, measured as UV-Vis signal at 260 nm.

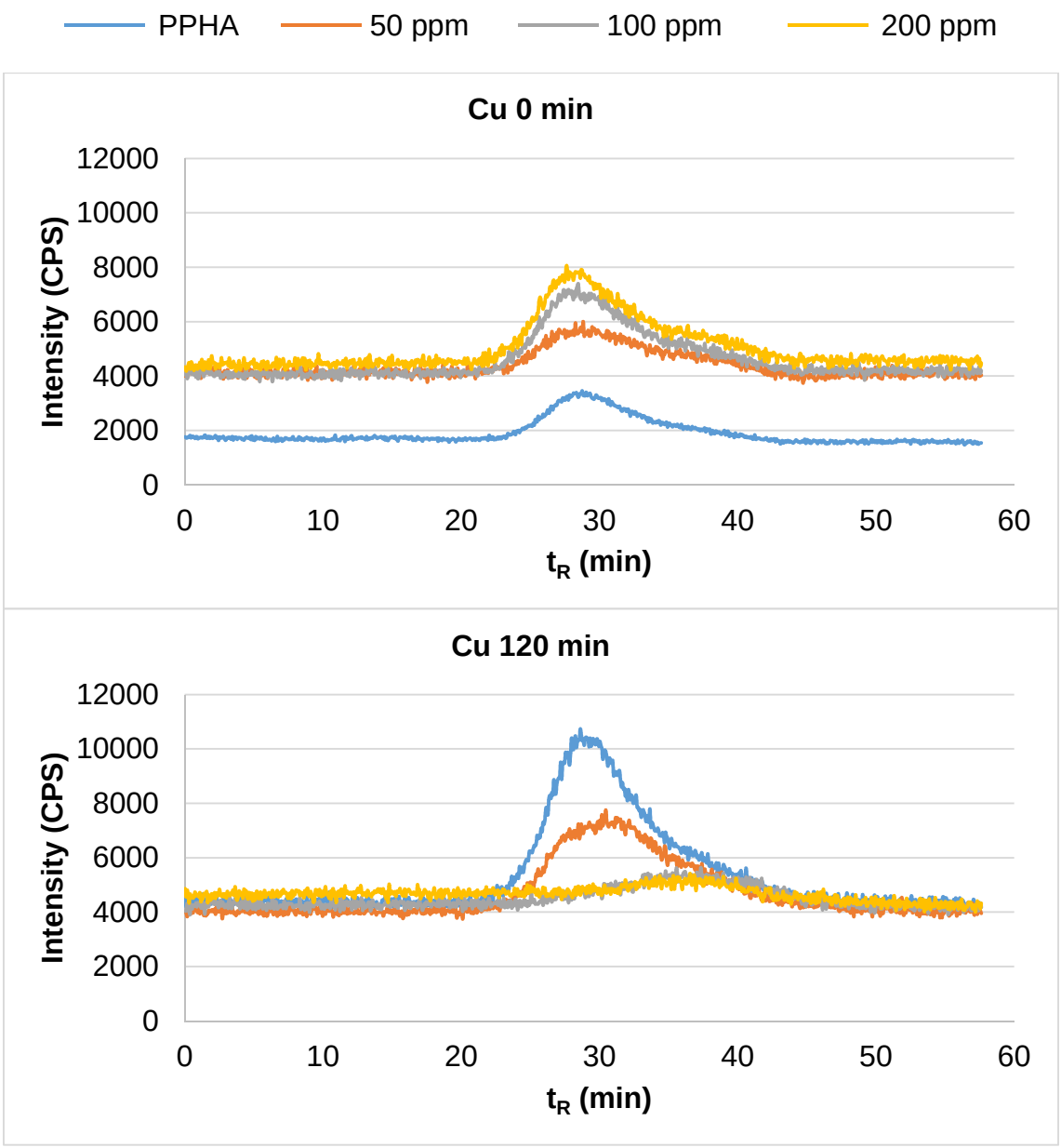

Figure 25 HPSEC – ICP-MS chromatograms for Copper, measured as UV-Vis signal at 260 nm.

With the calibration curves, the CPS were converted to µg/L. The flow rate (F_c) for these experiments was 0.3 mL/min. The sample injection volume was 0.2 mL. The retention time (t_R) was converted to retention volume (V_R) by multiplying it with the carrier flowrate, after subtracting the time taken by the sample to

reach from the system through post-column tubing to the detector flowcell (2.45 min).

The retention volume is defined as the volume of mobile phase necessary to convey a solute from the point of injection, through the column, and to the detector:

$$V_R = t_R F_c$$

Figure 26 shows the PPHA blank before irradiation (Ads), and after 120 min of irradiation. PPHA blank showed changes in the element signal after irradiation, while the change was less visible in the UV-Vis and Fluorescence analysis (Appendix Fig. 33). Al was not present before irradiation, but after 120min it appeared at 11 mL of retention volume, which corresponds to molecular weights smaller than 1100 g/mol. Fe, Ni and Cu were present at around 9 mL, associated to molecular weights of 7500 g/mol.

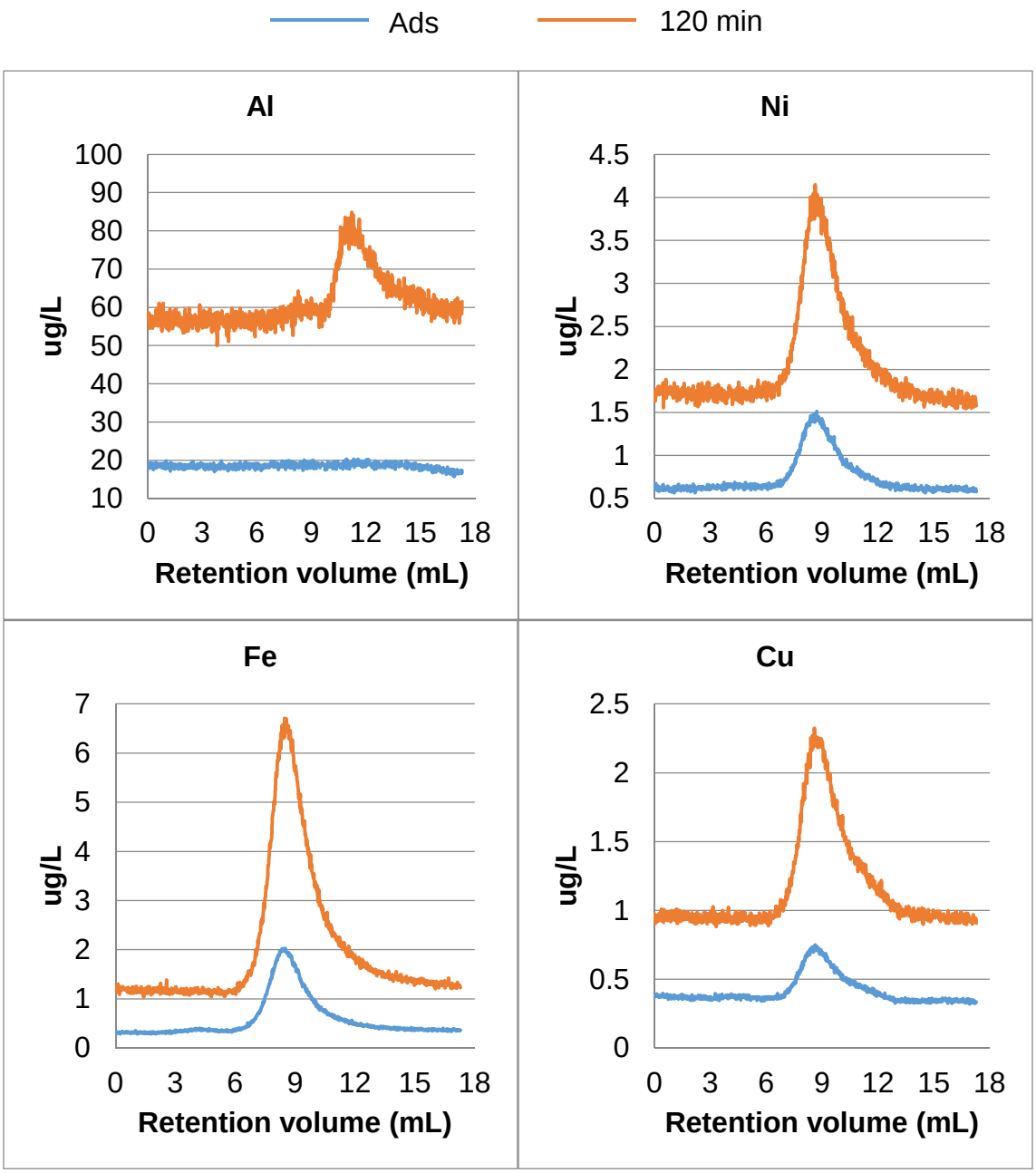

Figure 26 Element composition of PPHA before and after irradiation, without TiO_2.

Figure 27 shows the sample with 50 ppm of TiO_2 before irradiation (Ads), and after 120 min of irradiation. Al was associate with MW smaller than 1100 g/mol, and it only appeared after irradiation. Fe shifted slightly from 9.29 mL (7680

g/mol) to 9.40 mL (6795 g/mol), and there was an increase in the concentration. Ni shifted from 9.07 mL (9750 g/mol) to 10.02 mL (3438 g/mol), but the concentration remained almost the same. Cu shifted from 9.30 mL (7591 g/mol) to 9.85 mL (4142 g/mol), with an increase in concentration.

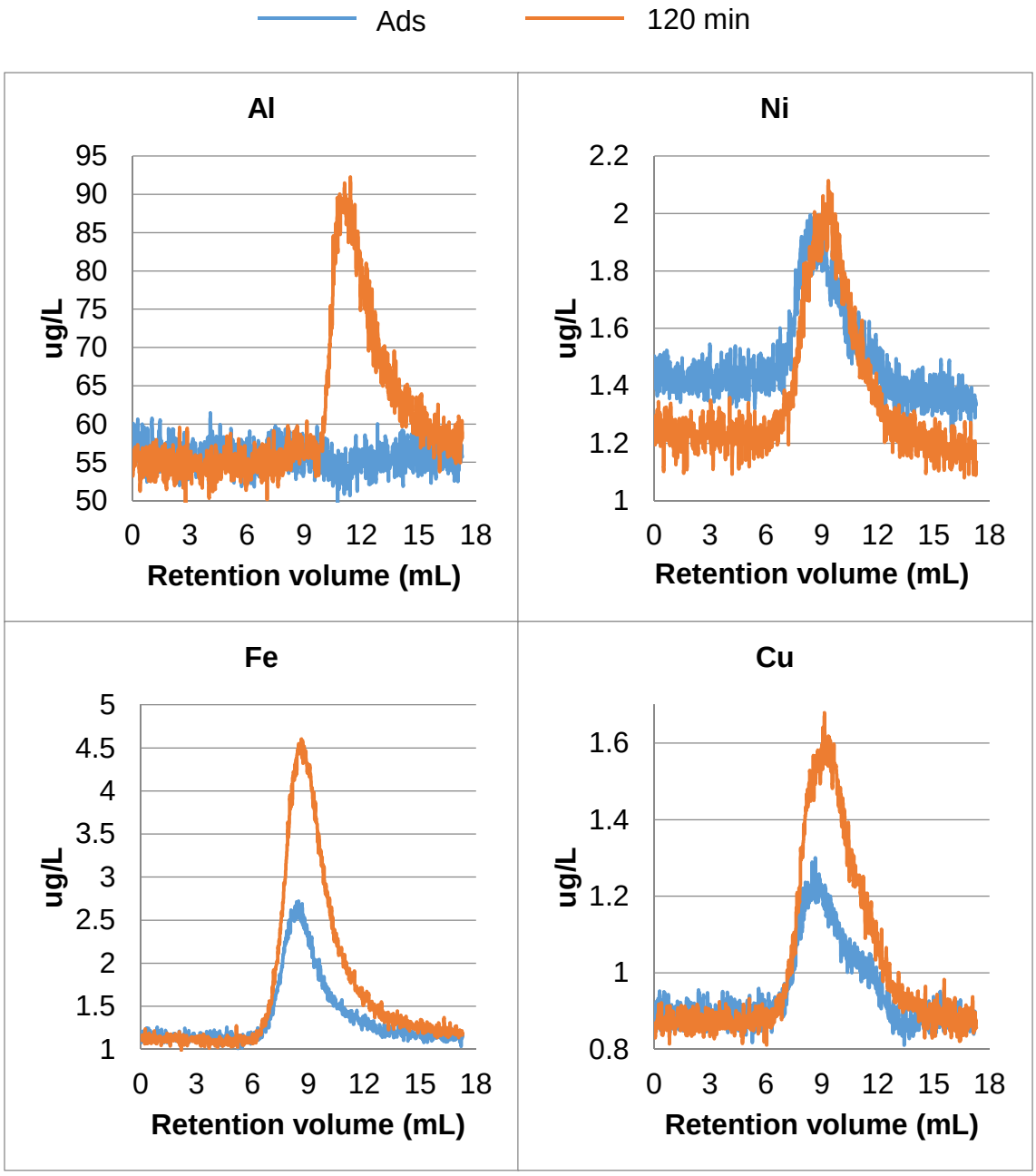

Figure 27 Element composition of PPHA before and after irradiation, with 50 ppm TiO_2

Figure 28 shows the sample with 100 ppm of TiO_2 before irradiation (Ads), and after 120 min of irradiation. Al appeared at 12.04 mL (376 g/mol) after irradiation. Fe shifted slightly from 9.16 mL (8831 g/mol) to 10.03 mL (3400 g/mol), and there was big increased in the concentration. Ni started at 9.21 mL (8380 g/mol), and after 120 min irradiation the peak almost disappeared. Cu shifted from 9.26 mL (7860 g/mol) to 10.35 mL (2393 g/mol), with a decrease in concentration.

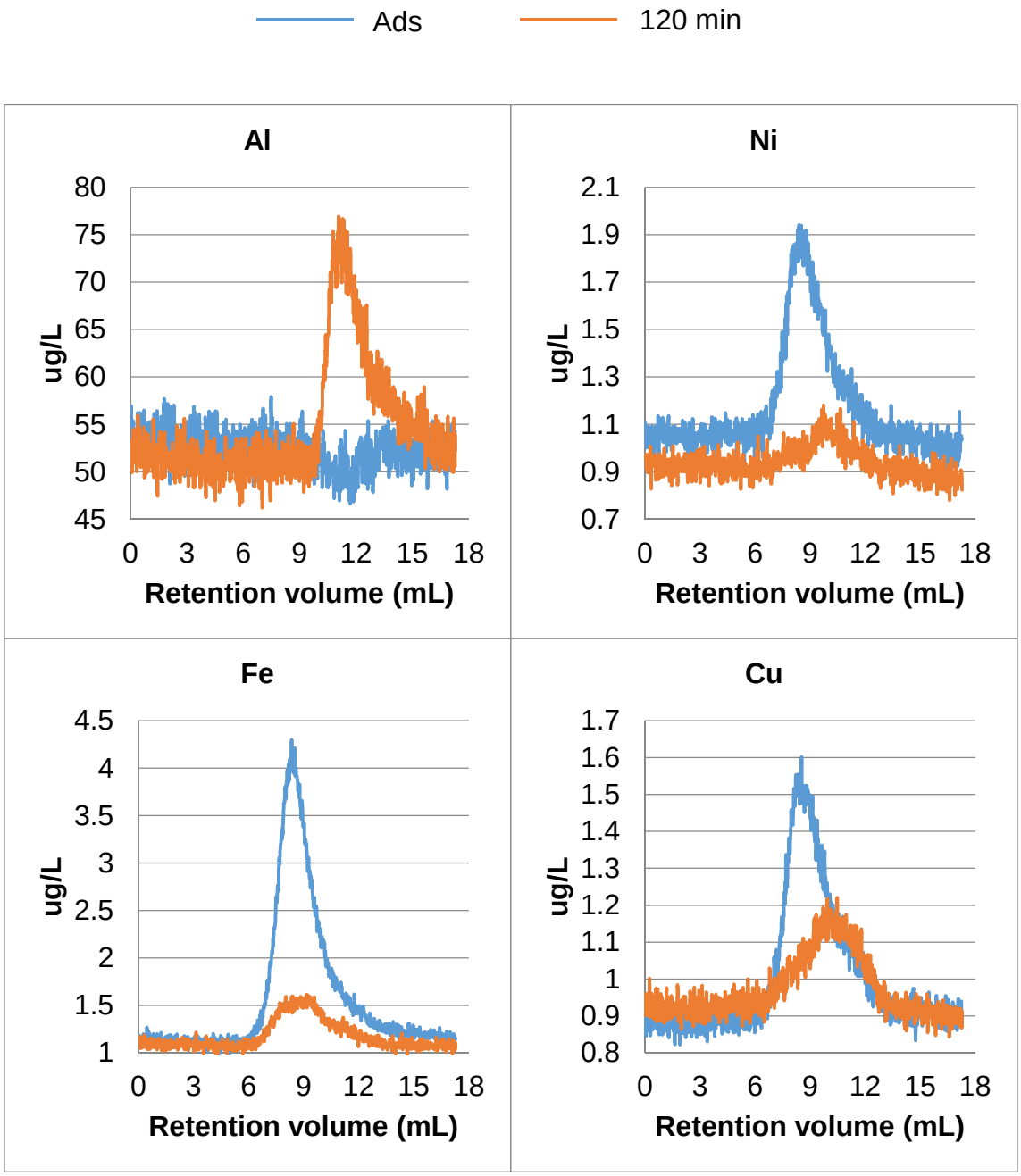

Figure 28 Element composition of PPHA before and after irradiation, with 100 ppm TiO_2

Figure 29 shows the sample with 200 ppm of TiO_2 before irradiation (Ads), and after 120 min of irradiation. Al did not appear in the samples. Fe, Ni and Cu appeared at 9.00 mL (10455 g/mol) and their signals were lost after 120 min of irradiation.

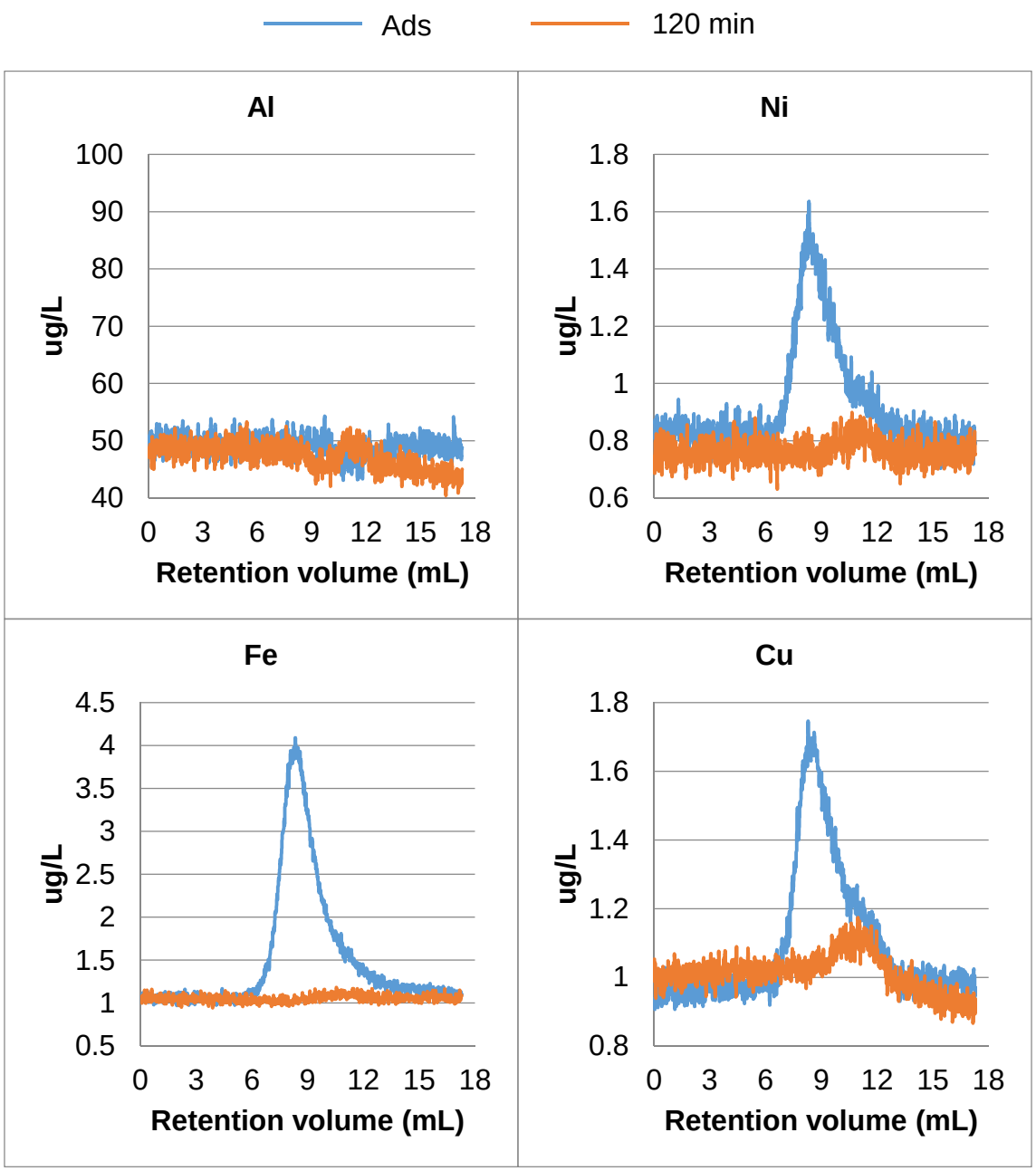

Figure 29 Element composition of PPHA before and after irradiation, with 200 ppm TiO_2

4. Conclusions and Outlook

The results of this thesis showed that the photocatalytic TiO_2 nanoparticles produce changes in the UV-Vis absorbance, fluorescence, molecular weight distribution and element distribution in the PPHA molecule. However, this changes are influenced differently by the initial TiO_2 concentration, which affects the adsorption and therefore, the photodegradation mechanism. A correlation between TiO_2 concentration and degradation intensity could not be made, which gives a hint about the complexity of this process.

The efficiency of this process depends on several factors, including light intensity, wavelength, initial humic acid concentration, pH and crystal structure of TiO_2. This parameters have to be chosen at the beginning of the experiment, and will further determine the results. In the experiments, TiO_2 had high photocatalytic activity.

Gross parameters, such as UV_{260} and fluorescence, could give a general evaluation on mineralization and overall loss of UV absorbing moieties, but they do not elucidate the chemistry of the process in any detail. Thus, with the use of HPSEC-UV—Vis-fluorescence-ICP-MS, it was possible to gain insight on the apparent molecular weight and the association of elements of humic acids, and NOM in general, at different stages of the photocatalytic degradation process.

The photocatalytic degradation reduced potential of formation of THMs and DBPs, as confirmed by absorbance ratios.

The large aromatic and long aliphatic chain molecules were degraded into lower molecular weight organics. Aluminum was associated to low molecular weight particles, while iron, nickel and copper were associated with higher molecular weight particles. Irradiation changes in the molecule with the absence of TiO_2 were only visible with the elemental distribution, but this is believed to be an interference of the glassware. Analysis of elements in solution would be helpful to understand better their transfer between humic acid particles and the solution.

The results of this thesis could be followed by adding a complete mass balance of the humic acid, since it was only possible to analyze the fraction left in solution and not the fraction adsorbed onto the surface of TiO2. However, a technique to analyze the absorbed fraction would be necessary. Only then, we would have a more comprehensive understanding of the degradation process.

5. Acknowledgements

I would like to express my gratitude to Dr. Frank von der Kammer for proposing this topic and sharing his great knowledge with me. To Dr. Jana Navratilova for helping me in any way she could.

To my friends Judith, Karo, Franzis, Stefan&Conny, Ekaterina and Bernadette. I could not thank you enough for your constant support and for always being there when I needed you most. For your invaluable advices, for our great times together and for making all of this worth it.

To my many Familie in Vienna: F. Kreitner, F. Bauchinger, F. Waldherr and F. Nebel, for giving me a warm and loving place in your homes, and delicious, heartwarming food.

To all the people I've met in Vienna that have a place in my heart, Stef, Samira, Lukas, Angelika, and many more people that contributed to my happiness.

Most of all, to my mother, because she is the strongest, more courageous woman I have ever know, she is the reason behind all of this. Te amo madrecita.

6. References

Abbt-Braun, G., Lankes, U., Frimmel, F.H. (2004) Structural characterization of aquatic substances – The need for a multiple method approach. Aquat. Sci. 66: p. 151-170.

Bekbolet, M., Suphandag, A.S., Uyguner, C.S (2002) An investigation of the photocatalytic efficiencies of TiO2 powders on the decolorisation of humic acids. Journal of Photochemistry and Photobiology A: Chemistry 148: p. 121-128.

Bieroza, M., Baker, A., Bridgeman, J. (2009) Relating freshwater organic matter fluorescence to organic carbon removal efficiency in drinking water treatment. Science of the Total Environment 47: p. 1765-1774.

Carp, O., Huisman, C.L., Reller, A. (2004) Photoinduced reactivity of titanium dioxide. Progress in Solid State Chemistry 32: p. 33-177.

Chen, C., Zhang, X., Zhu, L., Liu, J., He, W., Han, H. (2008) Desinfection by-products and their precursors in a water treatment plant in North China: seasonal changes and fraction analysis. Sci. Total Environ. 397: p. 140-147.

Chen, J., Gu, B., LeBoeuf, E.J., Pan, H., Dai, S. (2002) Spectroscopic characterization of the structural and functional properties of natural organic matter fractions. Chemosphere 48: p. 59-6.

Cui, X., Choo, K-H. (2014) Natural Organic Matter Removal and Fouling Control in Low-Pressure Membrane Filtration for Water Treatment. Environ. Eng. Res. March, 19(1): p. 1-8.

Erhayem, M., Sohn, M. (2014) Effect of humic acid source on humic acid adsorption onto titanium dioxide nanoparticles. Science of the Total Environment 470-471: p. 92-98.

Foo, K.Y., Hameed, B.H. (2010) Insights into the modeling of adsorption isotherm systems. Chemical Engineering Journal 156: p. 2–10.

Ibrahim, N., Aziz, H. A. (2014) Trends on Natural Organic Matter in Drinking Water Sources and its Treatment. International Journal of Scientific Research in Environmental Sciences, 2(3): p. 94-106.

JRC Repository: NM-Series of Representative Manufactured Nanomaterials (2014) Titanium Dioxide, NM-100, NM-101, NM-102, NM-103, NM-104, NM-105: Characterization and Physico-Chemical Properties.

Kim, H.C., Yu, M.J. (2007) Characterization of aquatic humic substances to DBPs formation in advanced treatment processes for conventionally treated water. Journal of Hazardous Materials 143: p. 486-493.

Kördel, W., Dassenakis, M., Lintelmann, J., Padberg, S. (1997) The importance of Natural Organic Material for environmental processes in water and soils. Pure and Applied Chemistry 69(7): p. 1571-1600.

Kumke, M.U., Specht, C.H., Brinkmann, T., Frimmel, F.H. (2001) Alkaline hydrolysis of humic substances – spectroscopic and chromatographic investigations. Chemosphere 45: p. 1023-1031.

Limousin, G., Gaudet, J.P., Charlet, L., Szenknect, S., Barthès, V., Krimissa, M. (2007) Sorption isotherms: A review on physical bases, modeling and measurement. Applied Geochemistry 22: p. 249-275.

Ljubas, D. (2005) Solar photocatalysis – a possible step in drinking water treatment. Energy 30: p. 1699-1710.

Matilainen, A., Gjessing E.T., Lahtinen, T., Leif, H., Bhatnagar, A., Sillanpää, M. (2011) An overview of the methods used in the characterization of natural organic matter (NOM) in relation to drinking water treatment. Chemosphere 83: p. 1431-1442.

Matilainen, A., Sillanpää, M. (2010) Removal of natural organic matter from drinking water by advanced oxidation processes. Chemosphere 80: p. 351-365.

Neubauer, E., v.d.Kammer, F., Hofmann, T. (2013) Using FLOWFFF and HPSEC to determine trace metal colloid associations in wetland runoff. Water Research 47: p. 2757-2769

O'Loughlin, E., Chin, Y-P. (2001) Effect of detector wavelength on the determination of the molecular weight of humic substances by High-Pressure Size Exclusion Chromatography. Wat. Res. 35(1): p. 333-338.

Palmer, F.L., Eggins, B.R., Coleman, H.M. (2002) The effect of operational parameters on the photocatalytic degradation of humic acid. Journal of Photochemistry and Photobiology A: Chemistry 148: p. 137-143.

Pansamut, G., Charinpanitkul, T., Suriyawong, A. (2013) Removal of Humic Acid by Photocatalytic Process: Effect of Light Intensity. ENGINEERING JOURNAL 17(3): p. 25-32.

Tercero, L.A., Haseborg, E.T., Weber, M., Frimmel, F.H. (2009) Investigation of photocatalytic degradation of brown water natural organic matter by size exclusion chromatography. Applied Catalysis B: Environmental 87: p. 56-62.

Thiruvenkatachari, R., Vigneswaran, S., Moon, I.S. (2008) A review on UV/TiO_2 photocatalytic oxidation process. Korean J. Chem. Eng., 25(1): p. 64-72.

Toyoda, M., Nanbu, Y., Nakazawa, Y., Hirano, M., Inagaki, M. (2004) Effect of crystallinity of anatase on photoactivity for methyleneblue decomposition in water. Applied Catalysis B: Environmental 49: p. 227-232.

Tryba, B., Toyoda, M., Morawski, A.W., Nonaka, R., Inagaki, M. (2007) Photocatalytic activity and OH radical formation on TiO_2 in the relation to crystallinity. Applied Catalysis B: Environmental 71: p. 163-168.

Uyguner, C. S., Bekbolet, M. (2005a) Evaluation of humic acid photocatalytic degradation by UV-Vis and fluorescence spectroscopy. Catalysis Today 101: p. 267-274.

Uyguner, C. S., Bekbolet, M. (2005b) Implementation of spectroscopic parameters for practical monitoring of natural organic matter. Desalination 176: p. 47-55.

Uyguner-Demirel, C.S., Bekbolet, M. (2011) Significance of analytical parameters for the understanding of natural organic matter in relation to photocatalytic oxidation. Chemosphere 84: p. 1009-1031.

Valencia (2012) Study of pH effects on the evolution of properties of brown-water natural organic matter as revealed by size-exclusion chromatography during photocatalytic degradation. Water Science 46: p. 1198-1206.

Valencia, S., Marín, J.M., Restrepo, G., Frimmel, F.H. (2013) Application of excitation-emission fluorescence matrices and UV/Vis absorption to monitoring the photocatalytic degradation of commercial humic acid. Sciences of the Total Environment 442: p. 207-214.

Xiaoju (2012) The Roles of Hydroxyl Radicals, Photo-Generated Holes and Oxygen in the Photocatalytic Degradation of Humic Acid. Russian Journal of Physical Chemistry A 86(9): p. 1479-1485.

Zhou, Q., Cabaniss, S.E., Maurice, P.A. (2000) Considerations in the use of High-Pressure Size Exclusion Chromatography (HPSEC) for determining molecular weight of aquatic humic substances. Water Research 34(14): p. 3505-3514.

http://heraeus-quarzglas.com/en/quarzglas/chemicalpurity/Chemical_purity.aspx

7. Appendix

Table 4 Chemical properties of 1R103H Pahokee Peat reference humic acid. Source: © 2015 International Humic Substances Society

Elemental composition									
H_2O	Ash	C	H	O	N	S	P	^{13}C	^{15}N
10.4	1.72	56.84	3.60	36.62	3.74	0.70	0.03	-26.3	1.43
Acidic functional groups				**Amino Acid content**			**Carbohydrate content**		
Carboxyl		Phenolic		360			98.1		
8.87		2.05							

H_2O content is the %(w/w) of H2O in the air-equilibrated sample (a function of relative humidity).

Ash is the %(w/w) of inorganic residue in a dry sample.

C, **H**, **O**, **N**, **S**, and **P** are the elemental composition in %(w/w) of a dry, ash-free sample.

$\delta^{13}C$ and **$\delta^{15}N$** are the abundances of the respective stable isotopes in units of per mil, or o/oo.

Carboxyl is the charge density (meq/g C) at pH 8.0; **Phenolic** is two times the change in charge density (meq/g C) between pH 8.0 and pH 10.0.

Concentration of amino acids are in units of µmol/g.

Concentration of carbohydrates are in units of µmol/g.

Time study

In order to determine the time at which the equilibrium of PPHA/TiO_2 suspension is attained, a 100 ml solution of PPHA (20 mg C/L at pH 4.5) and 0.5 g/L of TiO_2 was prepared. The sample was place in a stirring plate for 96 h. 10 ml subsamples were taken at regular intervals of time and centrifuged at 7000 rpm for 30 minutes, to precipitate and separate TiO_2 nanoparticles. Samples were measured with the Fluorescence Spectrometer, using an Excitation/Emission

wavelength of 425/550 nm, corrected with the blank signal, and converted to mg C/L.

Figure 30 shows the Equilibrium between PPHA and TiO_2. The Equilibrium was reached very early after the addition of the nano-TiO_2. Further, no significant additional adsorption of PPHA occurred after 5 minutes, as data shows. This result was in good agreement with previous research by Valencia et al. (2013) in which it was determined that the adsorption equilibrium of Aldrich HA onto TiO_2 in the dark was reached in less than 5 min. For all subsequent experiments, an adsorption time of 30 minutes was chosen to ensure saturation.

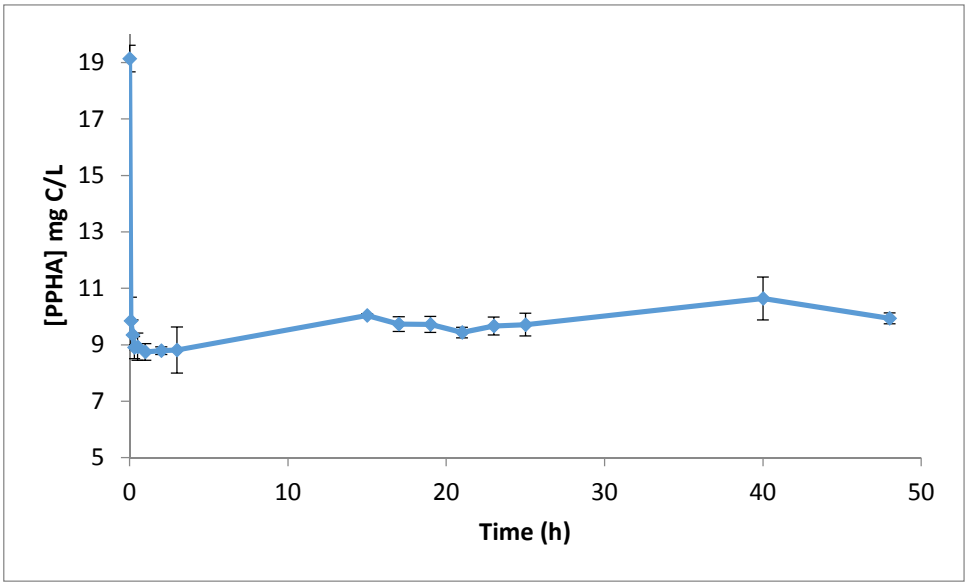

Figure 30 Equilibrium TiO_2-PPHA

Adsorption Isotherm data

An adsorption experiment was performed increasing the number of points in the curve. The results are as follow:

Table 5 Adsorption Isotherm data

	[HA] (mg C/l)	mT_{HA} (mg C)	f_{HA-w}	m_{HA-w} (mg C)	$f_{HA-TiO2}$	$m_{HA-TiO2}$ (mg C)	Vw (l)	C_{HA-w} (mg C/l) C_e	C_{TiO2} (g/l)	M_{TiO2} (g)	$C_{HA-TiO2}$ (mg C/g) q_e	Kd	%Adsorption
E1	19.781	0.396		0.396		0.000	0.020	19.781	0.000	0.000	#¡DIV/0!	#######	0.000
E2	19.781	0.396		0.261		0.134	0.020	13.061	0.100	0.002	67.196	5.145	33.970
E3	19.781	0.396		0.214		0.182	0.020	10.680	0.150	0.003	60.671	5.681	46.008
E4	19.781	0.396		0.209		0.187	0.020	10.450	0.200	0.004	46.653	4.464	47.169
E5	19.781	0.396		0.190		0.205	0.020	9.513	0.250	0.005	41.071	4.317	51.908
E6	19.781	0.396		0.173		0.223	0.020	8.634	0.300	0.006	37.155	4.303	56.350
E7	19.781	0.396		0.165		0.230	0.020	8.259	0.350	0.007	32.918	3.986	58.246
E8	19.781	0.396		0.138		0.257	0.020	6.918	0.400	0.008	32.156	4.648	65.025
E9	19.781	0.396		0.142		0.254	0.020	7.084	0.450	0.009	28.215	3.983	64.187
E10	19.781	0.396		0.126		0.269	0.020	6.316	0.500	0.010	26.930	4.264	68.071
E11	19.781	0.396		0.119		0.276	0.020	5.967	0.550	0.011	25.115	4.209	69.833
E12	19.781	0.396		0.107		0.289	0.020	5.355	0.600	0.012	24.043	4.489	72.927
E13	19.781	0.396		0.088		0.308	0.020	4.400	0.650	0.013	23.663	5.378	77.758
E14	19.781	0.396		0.083		0.312	0.020	4.161	0.700	0.014	22.315	5.363	78.967
E15	19.781	0.396		0.064		0.332	0.020	3.198	0.750	0.015	22.110	6.913	83.831
E16	19.781	0.396		0.059		0.337	0.020	2.931	0.800	0.016	21.062	7.185	85.181
E17	19.781	0.396		0.050		0.345	0.020	2.516	0.850	0.017	20.312	8.074	87.282
E18	19.781	0.396		0.045		0.351	0.020	2.248	0.900	0.018	19.481	8.667	88.636
E19	19.781	0.396		0.043		0.353	0.020	2.133	0.950	0.019	18.577	8.710	89.218
E20	19.781	0.396		0.039		0.357	0.020	1.927	1.000	0.020	17.854	9.265	90.258

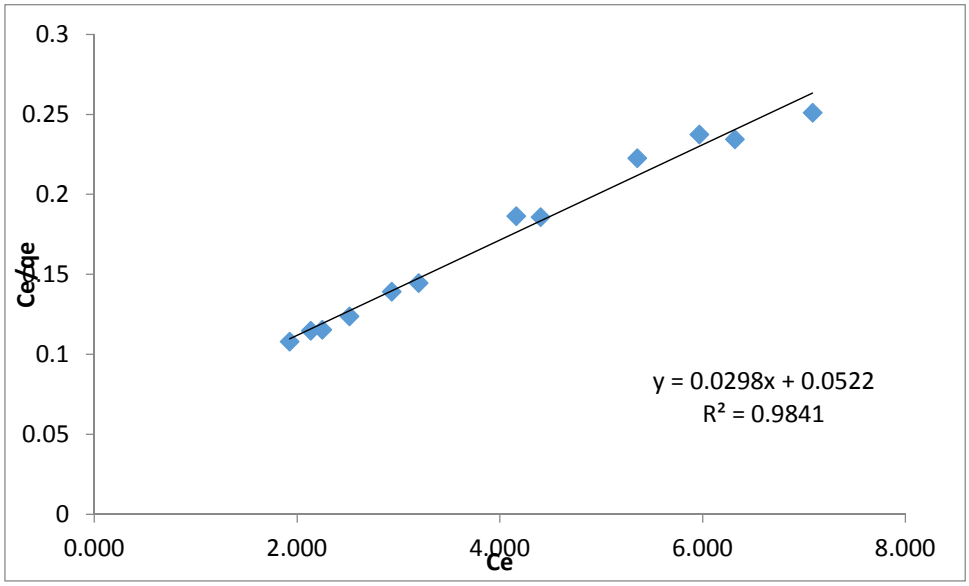

Figure 31 Langmuir fitting

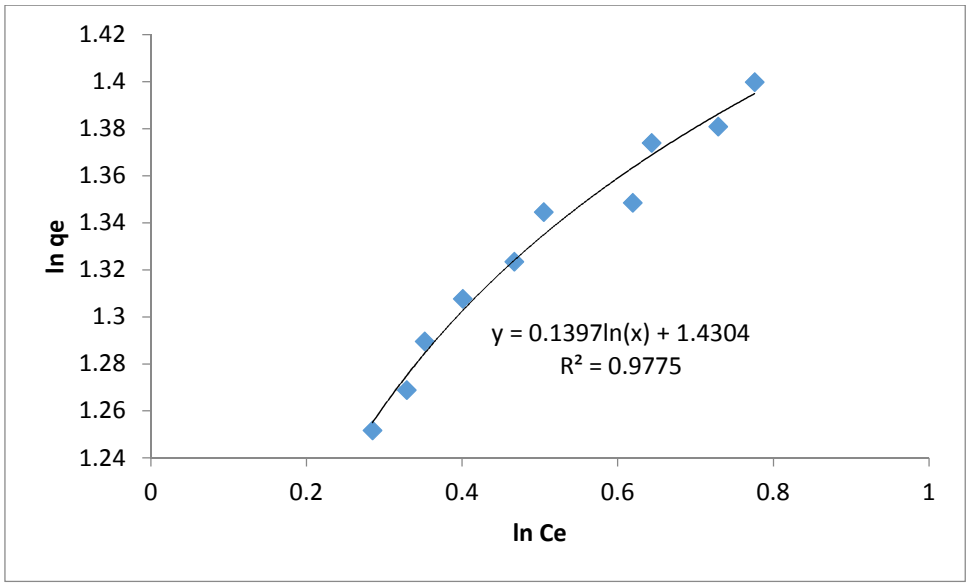

Figure 32 Freundlich fitting

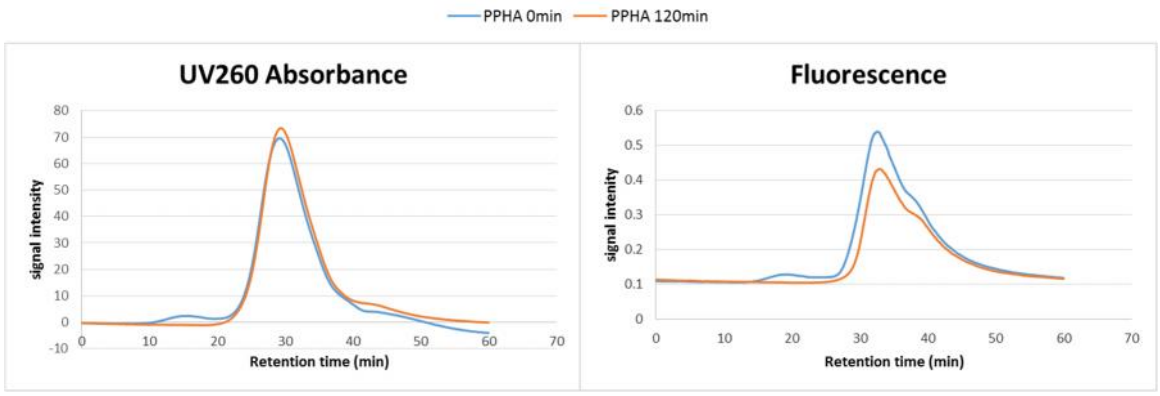

Figure 33 PPHA blank measured by HPSEC-UV--Vis-Fl

7.1. Statutory Declaration

I declare that I have authored this thesis independently, that I have hot used other that the declared sources/resources, and that I have explicitly marled all material which has been quoted either literally or by content from the used sources.

Vienna, _____ _____

Date Signature

7.2. Eidesstattliche Erklärun

Ich erkläre an Eides statt, dass ich die vorliegende Arbeit selbständig verfasst, andere als die angegebenen Quellen/Hilfsmittel nicht benutzt, und die den benutzten Quellen wörtlich und inhaltlich entnommenen Stellen als solche kenntlich gemacht habe.

Wien, am _____ _____

Datum Unterschrift